(4)

TECHNICAL REPORT BRL-TR-3015

BRL

JET-FLOW FROM SHOCK TUBES

CHARLES N. KINGERY
EDMUND J. GION

JULY 1989

U.S. ARMY LABORATORY COMMAND

BALLISTIC RESEARCH LABORATORY
ABERDEEN PROVING GROUND, MARYLAND

DESTRUCTION NOTICE

Destroy this report when it is no longer needed. DO NOT return it to the originator.

Additional copies of this report may be obtained from the National Technical Information Service, U.S. Department of Commerce, Springfield, VA 22161.

The findings of this report are not to be construed as an official Department of the Army position, unless so designated by other authorized documents.

The use of trade names or manufacturers' names in this report does not constitute indorsement of any commercial product.

SECURITY CLASSIFICATION OF THIS PAGE

REPORT DOCUMENTATION PAGE

Form Approved OMB No. 0704-0188

1a. REPORT SECURITY CLASSIFICATION UNCLASSIFIED	1b. RESTRICTIVE MARKINGS NONE
2a. SECURITY CLASSIFICATION AUTHORITY	3. DISTRIBUTION/AVAILABILITY OF REPORT Approved for public release; distribution is unlimited
2b. DECLASSIFICATION/DOWNGRADING SCHEDULE	
4. PERFORMING ORGANIZATION REPORT NUMBER(S) BRL-TR-3015	5. MONITORING ORGANIZATION REPORT NUMBER(S)
6a. NAME OF PERFORMING ORGANIZATION U. S. Army Ballistic Research Laboratory (BRL)	6b. OFFICE SYMBOL (If applicable) SLCBR-TBD
6c. ADDRESS (City, State, and ZIP Code) Aberdeen Proving Ground, MD 21005-5066	7a. NAME OF MONITORING ORGANIZATION
8a. NAME OF FUNDING/SPONSORING ORGANIZATION DOD Explosives Safety Board	8b. OFFICE SYMBOL (If applicable)
8c. ADDRESS (City, State, and ZIP Code) 2461 Eisenhower Ave. Alexandria, VA 22331-0600	7b. ADDRESS (City, State, and ZIP Code)
	9. PROCUREMENT INSTRUMENT IDENTIFICATION NUMBER
	10. SOURCE OF FUNDING NUMBERS PROGRAM ELEMENT NO. / PROJECT NO. 4A66 580 5M85 / TASK NO. / WORK UNIT ACCESSION NO.

11. TITLE (Include Security Classification)

Jet-Flow from Shock Tubes

12. PERSONAL AUTHOR(S)
Charles N. Kingery and Edmund J. Gion

13a. TYPE OF REPORT	13b. TIME COVERED	14. DATE OF REPORT (Year, Month, Day)	15. PAGE COUNT
BRL Technical Report	FROM Sept 87 TO July 88		

16. SUPPLEMENTARY NOTATION

17. COSATI CODES		
FIELD	GROUP	SUB-GROUP
20	04	
14	02	

18. SUBJECT TERMS (Continue on reverse if necessary and identify by block number)
Airblast; Overpressure; Shock Tube; Blast Waves; Stagnation pressure; Munition Storage; Exit Blast; Cube Displacement; Helium Driver

19. ABSTRACT (Continue on reverse if necessary and identify by block number)

This project was designed to map the magnitude and extent of the high velocity jet-flow exiting shock tubes. The flow was measured by installing stagnation probes along three blast lines and by supplementing these measurements with calibrated displacement cubes. The side-on and stagnation overpressure versus time were measured, and from that, the side-on and stagnation impulse were calculated. The stagnation impulse showed a large drop in magnitude as the blast line was moved from the zero line to a 1.5 and then to a 3-diameter offset. A helium driver was used in the 2.54-cm-diameter shock tube to simulate an explosion in a storage magazine. Results are presented in the form of stagnation impulse versus distance along the three blast lines. The significance of these findings is that the present quantity-distance criteria for munitions stored in underground magazines are based on side-on peak overpressure, but our results show that the peak stagnation pressure and impulse are much greater. At a distance where 10.3-kPa (1.5 psi) side-on pressure was measured, a 49.6-kPa (7.2 psi) stagnation pressure was measured. At the same distance, a side-on impulse was 12.6 kPa-ms (1.83 psi-ms), while the stagnation impulse was 134 kPa-ms (20.2 psi-ms)--a dramatic difference.

20. DISTRIBUTION/AVAILABILITY OF ABSTRACT	21. ABSTRACT SECURITY CLASSIFICATION
☒ UNCLASSIFIED/UNLIMITED ☐ SAME AS RPT. ☐ DTIC USERS	
22a. NAME OF RESPONSIBLE INDIVIDUAL Charles Kingery	22b. TELEPHONE (Include Area Code) (301) 272-4914 / 22c. OFFICE SYMBOL SLCBR-TBD

DD Form 1473, JUN 86 — Previous editions are obsolete. — SECURITY CLASSIFICATION OF THIS PAGE

TABLE OF CONTENTS

FIGURES

TABLES

1. INTRODUCTION

1.1 Background. The peak overpressure exiting from shock tubes, underground munition storage site tunnel models, and full-scale sites has been documented and reported in Reference 1. The criterion for structural damage is peak side-on overpressure.[2] Although it is well known that dynamic pressure and dynamic pressure impulse can be a primary damage mechanism, little is known about the propagation of dynamic pressure outside of a tube or tunnel. The dynamic pressure may cause more damage than the peak side-on overpressure. It is for this reason that the current program has been conducted by the BRL with funding from the DOD Explosives Safety Board.

1.2 Objectives. It is well known that a narrow, high-velocity flow exits shock tubes,[3] but the extent and magnitude are not well documented. One of the objectives of this study was to document the dynamic pressure and impulse propagating outside the tube along the zero degree axis. A second objective was to determine the width of the jet-flow by establishing off-set blast lines in units of tunnel diameter. The first blast line was along the zero axis; the second blast line was offset 1.5 tunnel diameters; and the third line was offset 3 tunnel diameters. We comment here that stagnation pressure impulse is taken to be equivalent to the dynamic pressure impulse because the side-on pressure impulse was found to be relatively insignificant in comparison.

A second method planned for mapping the magnitudes and extent of the jet-flow was to place small cubes of different density material in and out of the flow path and, from the measured displacement, to calculate the dynamic pressure impulse.

2. TEST PROCEDURES

2.1 Shock tube description. In order to conduct the experimental program in a controlled environment, a large open area in a BRL warehouse was established as the test site. A platform of 2.54-cm plywood on 5-cm by 15-cm (2 in x 6 in) wooden studs was constructed to facilitate gauge mounting and cable runs. A 2.54-cm (1-in) inside diameter, steel shock tube was selected because it would be operative indoors without resorting to remote control. A sketch of the tube is shown in Figure 1. The driver section of the tube was 150 cm (59 in), and the driven section was 133 cm (52.5 in). The wall thickness of the tube was 1.27 cm. If we consider a full size tunnel diameter of 5 m, then this tube is a 1:197 scale.

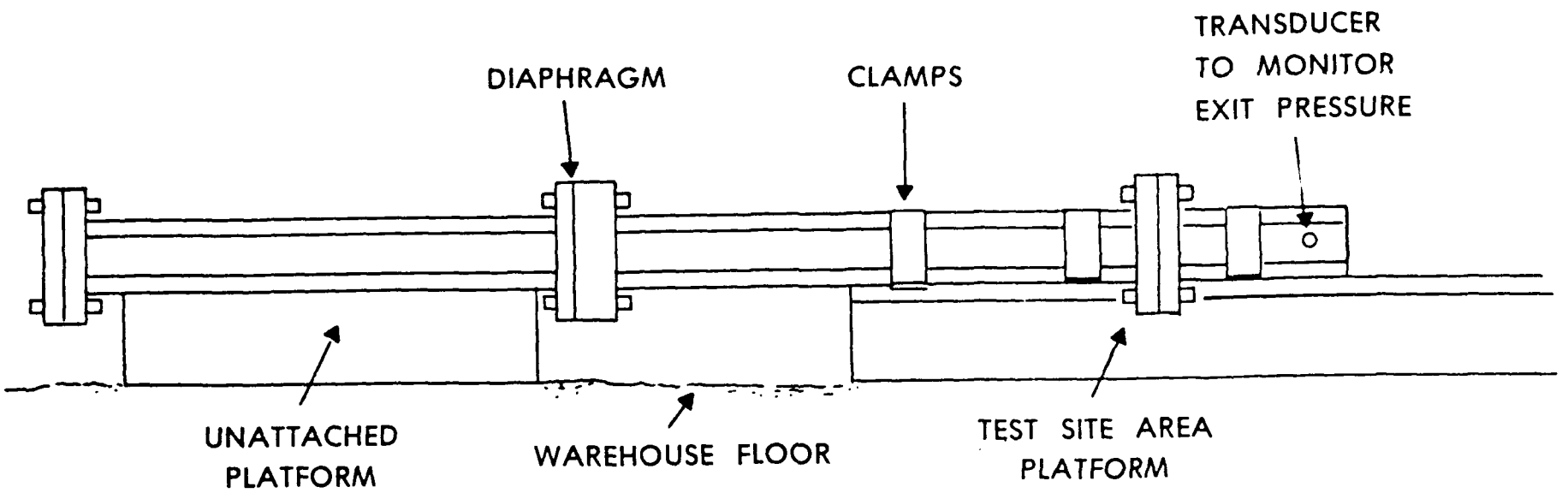

Figure 1. Sketch of 2.54-cm inside diameter shock tube.

2.2 Instrumentation description. A schematic of the data acquisition-reduction system is given in Figure 2. Quartz piezoelectric transducers were used to record both the side-on overpressure and stagnation pressure versus time. The transducers are coupled through a power supply and data amplifiers to a digitizing oscilloscope. On-site comparisons of the results were made directly from the hard copies of the pressure versus time records. Final data processing and generation of the overpressure and stagnation impulse versus time were completed with the computer, printer, and plotter.

The stagnation pressure was recorded using a stagnation probe, as shown in Figure 3. This type of transducer has been used successfully in many shock tube experiments. Because of the steel wool placed inside the probe to dampen reflections, there is a finite rise-time associated with the recorded stagnation pressure versus time record. This does not affect the primary flow measurements because of the long duration.

2.3 Transducer layout. It was surmised that the jet-flow extended a considerable distance beyond the tunnel exit but was rather narrow. Therefore, rather than mapping the area along different radial lines extending from the tunnel entrance--i.e. 0, 5, 10, 15 degrees--the decision was made to map with parallel lines. The parallel lines established were a zero offset, 1.5-tube diameter offset, and a 3.0-tube diameter offset. The offsets and transducer locations are shown in Figure 4. In reality, the offsets were achieved by moving the shock tube rather than by establishing new gauge lines. The location of the transducers was planned to produce a peak side-on overpressure of 5 kPa to 8 kPa at the last station for the different exit pressures. That is 35 diameters for the 500-kPa exit pressure, 48 diameters for the 900-kPa exit pressure, and 72 diameters for the 1,800-kPa exit pressure. The side-on and stagnation pressure both could not be made at each station on the same test; consequently, after one test, they were alternated, and a second test was conducted.

2.4 Cube displacement method. One method for measuring the flow effects is to measure the displacement of objects having known volume and density. A relationship between dynamic pressure impulse, displacement, initial velocity, and cube parameters can be summed up in the following equation.[4]

$$\Delta I_s = (w/C_D A g)\sqrt{\frac{D}{C}} \qquad (1)$$

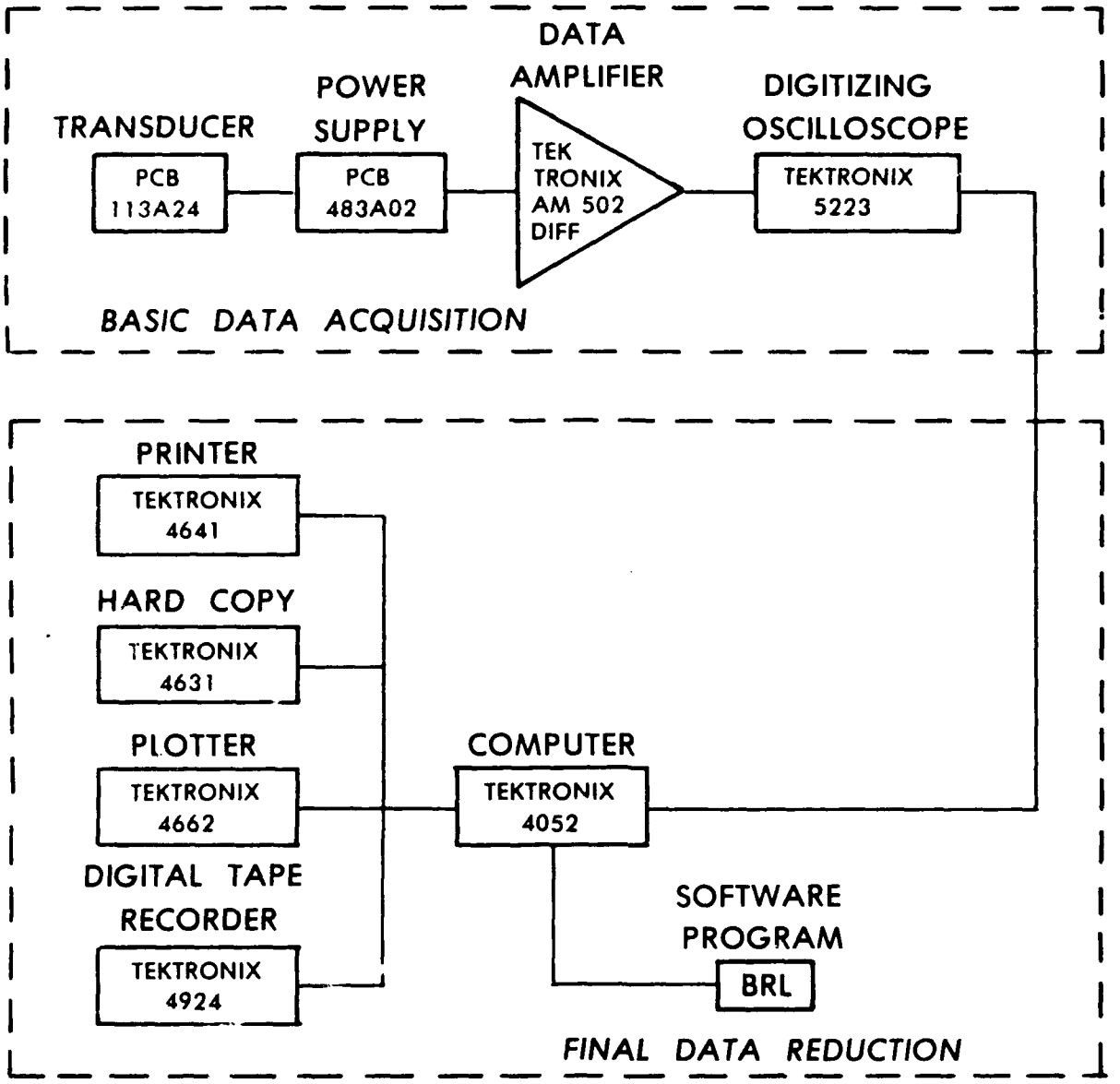

Figure 2. Schematic of data acquisition-reduction system.

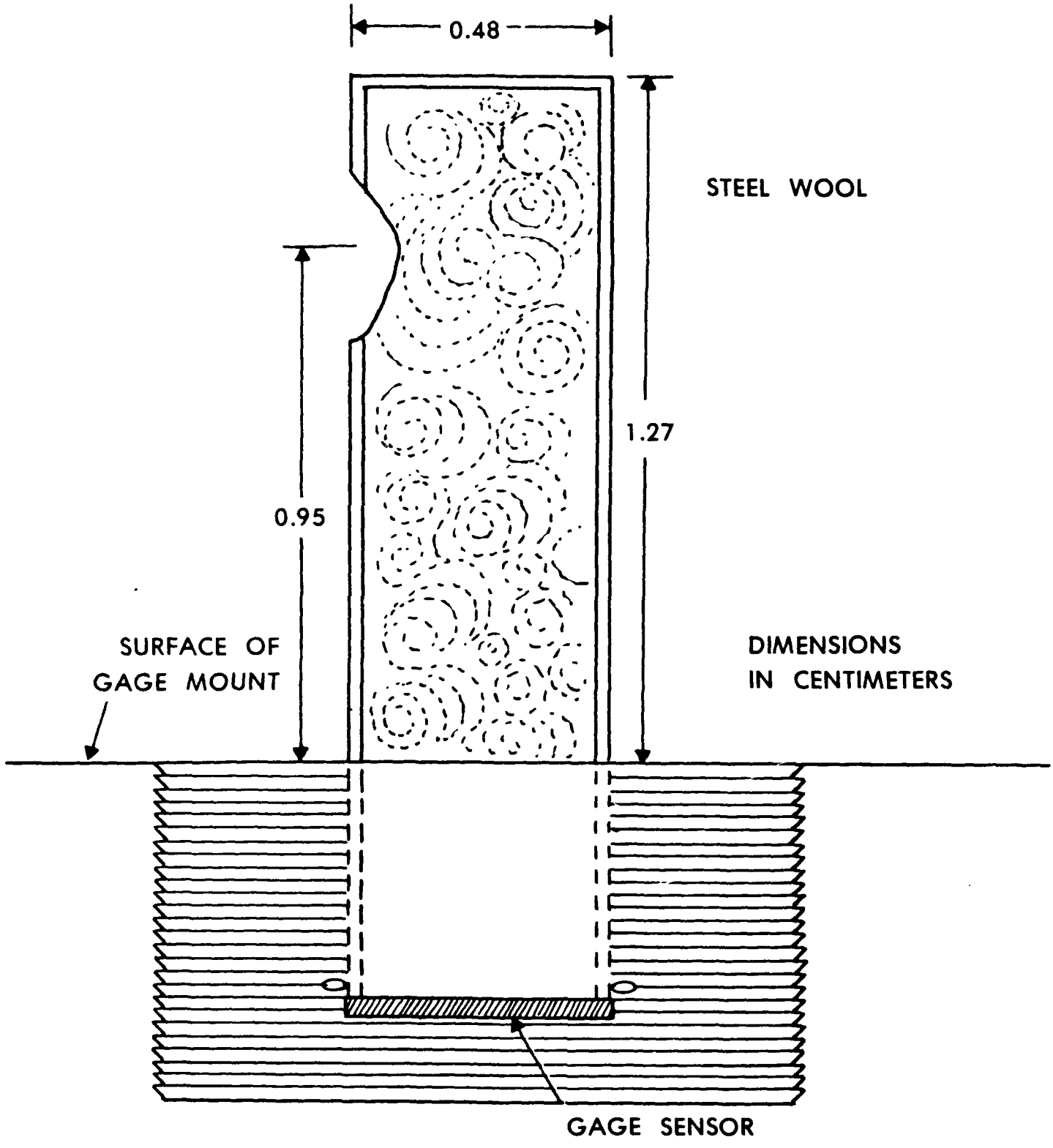

Figure 3. Sketch of stagnation probe.

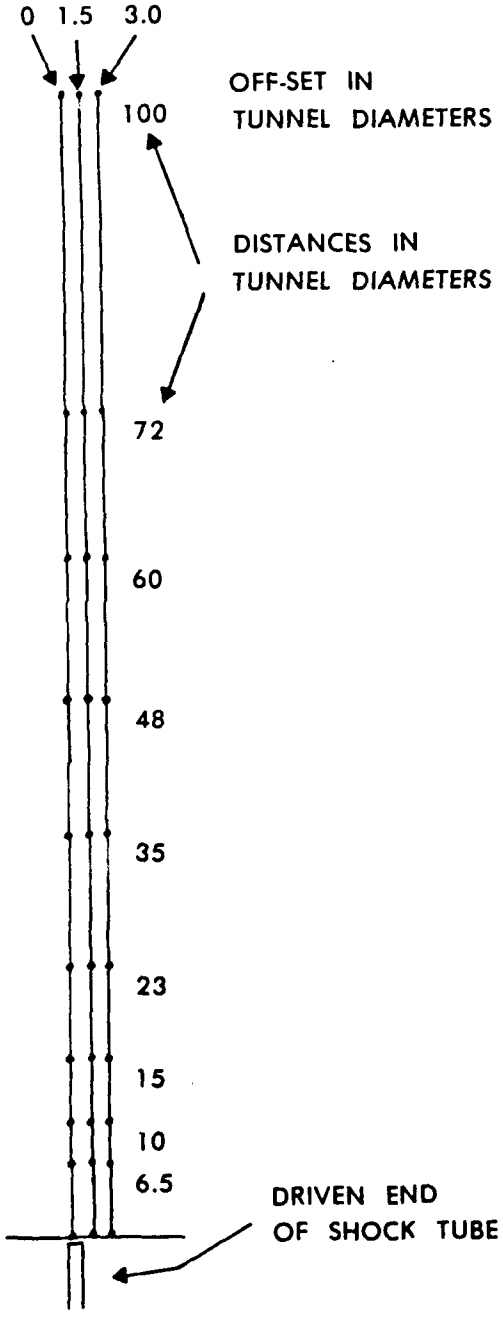

Figure 4. Transducer layout.

where

ΔI_s = stagnation pressure impulse,* kPa-ms

w = weight, (if mass of cube is given in kilograms, then w = kg x g)

C_D = Coefficient of drag, 1.2

A = cube face area, m^2

g = 9.80 m/sec^2

D = displacement, m

V_o = initial velocity, m/s

C = D/V_o^2, s^2/m**

For a given cube, W, C_D, A, g, and $\sqrt{C}$ can be lumped into one constant and Equation 1 becomes

$$\Delta I_s = k \sqrt{D}. \quad (2)$$

Along the zero offset line, the stagnation impulse (ΔI_s) has been documented; therefore, when the displacements for specific cubes are determined, the constant, k, can be obtained from

$$k = \Delta I_s / \sqrt{D}.$$

The values of k for the different cube materials will be given later.

3. RESULTS

3.1 Jet-flow generation. The jet-flow measured outside of a shock tube is a function of gas dynamics occurring within the driver section and driven section. In Figure 5, a wave diagram has been constructed to show the complicated interaction of the different gases and rarefaction waves. Because the density of the gas within the driver is important, helium was chosen as the driver gas to match as closely as possible the density of the driver gas when an explosion occurs in a storage chamber.

---

* Stagnation pressure impulse and dynamic pressure impulse are considered the same in this report.

**C was determined to be a constant based on the model described in Reference 4.

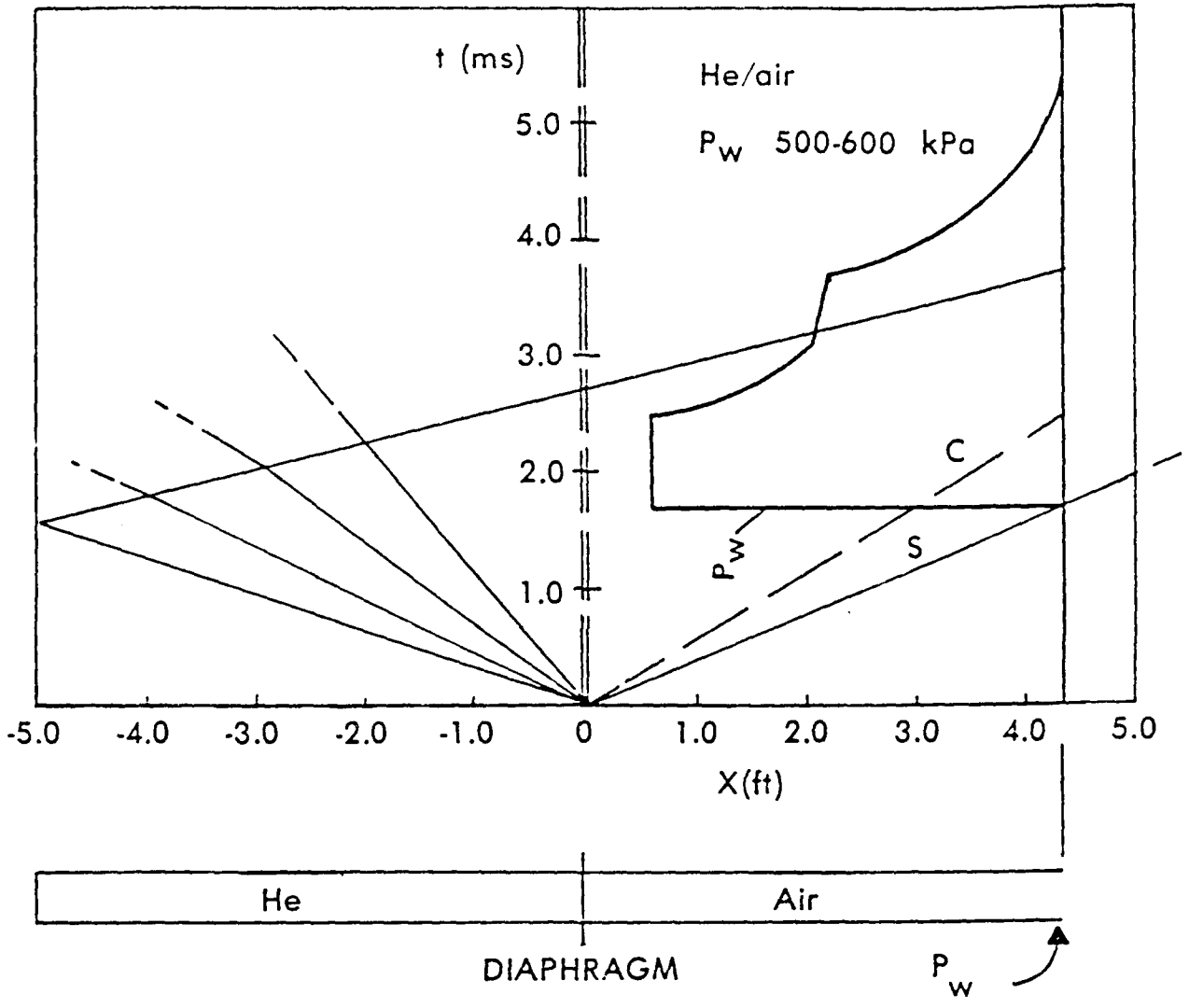

Figure 5. Wave diagram for exit pressure.

3.2 Transducer measurements. The peak side-on overpressure and stagnation pressure were both measured at the tube exit and along the zero and offset lines, but, because of reflections and blockage, they were not measured on the same shot. The primary objective of this program was to document the magnitude and extent of the jet-flow, and, therefore, most of the effort was expended in documenting the stagnation impulse. The station locations are shown in Figure 4. The two transducer stations not shown in Figure 4 are Station T-1 , located in the side wall of the tube at 2.54 cm from the end to measure the exit pressure and impulse--and Station S-1, a pilot-tube-type stagnation gauge with the sensing end 0.6 cm inside the exit to record the stagnation pressure and impulse versus time exiting the tube. A sketch of gauge and location is shown in Figure 6.

3.2.1 Results along the zero line. The stagnation impulses (ΔI_s) measured along the zero offset line are listed in Table 1. The values were first adjusted to account for variations in the exit impulse I_w. Exit impulse values of 1,500 kPa-ms, 5,000 kPa-ms, and 11,000 kPa-ms were selected as normalizing values. Therefore, if a stagnation impulse was measured from an exit impulse of 1,400 kPa-ms, it was multiplied by I_w 1,500/I_w 1,400 or 1.07 to bring it up to the norm. The values listed in Table 1 are average values from more than one test, and are plotted in Figure 7.

It was noted that the stagnation impulse (ΔI_s) values appeared to increase in proportion to the increase in the exit impulse I_w. The ratio of stagnation impulse (ΔI_s) along the zero off-set line to exit side-on impulse I_w are also listed in Table 1. The ratios $\Delta I_s/I_w$ listed in Table 1 are plotted in Figure 8 as $\Delta I_s/I_w$ versus R/D_T. The results can be represented by a single curve, with the exception of R/D_T of 10, where the 11,000 I_w value is lower than that for the other exit conditions. Based on this curve, values of (ΔI_s) along the zero line can be predicted for any side-on exit impulse ranging from 1,500 to 11,000 kPa-ms.

3.2.2 Results along the 1.5-diameter line. The stagnation impulses measured along the 1.5-diameter line for the three different pressure levels are listed in Table 2. The values are plotted in Figure 9. The stagnation impulses versus distance for the three pressure levels show similar trends, but the values of $\Delta I_s/I_w$ do not blend into a single curve when plotted as impulse ratios versus distance. Compared to the zero line, the curves in Figure 9 for the three input impulses show a dramatic decrease in stagnation impulse at the close-in stations 6.5, 10, and 15. Beyond station 23, the three curves show attenuation of impulse with distance. Beyond station 35, values of stagnation impulse at the 1.5-diameter offset appear to be the same as those measured along the zero line.

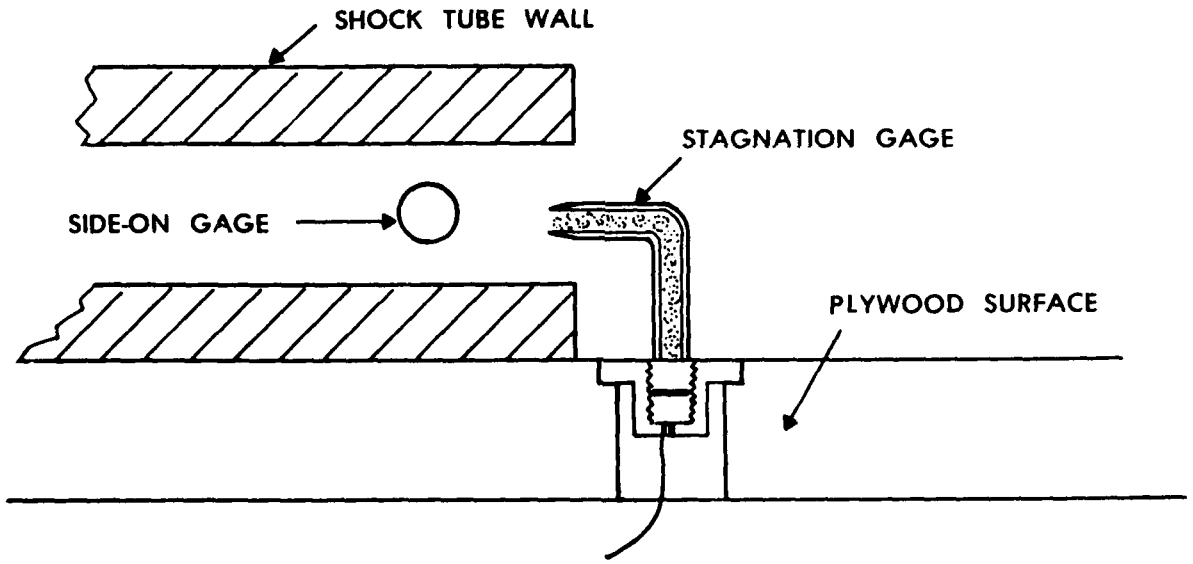

Figure 6. Sketch of stagnation probe at shock tube exit.

TABLE 1. Stagnation Impulse along the Zero Line.

Dist.	I_w=1,500 kPa-ms		I_w=5,000 kPa-ms		I_w=11,000 kPa-ms	
R/D_T	ΔI_s, kPa-ms	$\Delta I_s/I_w$	ΔI_s, kPa-ms	$\Delta I_s/I_w$	ΔI_s, kPa-ms	$\Delta I_s/I_w$
4.5	959	0.639	...	...	...	...
6.5	518	0.345	1,863	0.373	3,627	0.330
10.0	479	0.319	1,566	0.313	2,407	0.219
15.0	296	0.197	1,137	0.227	2,238	0.204
23.0	142	0.095	460	0.092	1,212	0.110
35.0	54	0.036	172	0.034	478	0.044
48.0	17	0.011	43	0.009	126	0.012
54.0	17	0.011	...	...	135	0.012
60.0	17	0.011	41	0.008	126	0.012

TABLE 2. Stagnation Impulse along the 1.5-Diameter Offset Line.

Dist.	I_w=1,500 kPa-ms		I_w=5,000 kPa-ms		I_w=11,000 kPa-ms	
R/D_T	ΔI_s, kPa-ms	$\Delta I_s/I_w$	ΔI_s, kPa-ms	$\Delta I_s/I_w$	ΔI_s, kPa-ms	$\Delta I_s/I_w$
4.5	49	0.032	155	0.031	...	...
6.5	87	0.058	117	0.023	368	0.034
10.0	72	0.048	192	0.039	511	0.047
15.0	86	0.057	270	0.054	608	0.055
23.0	99	0.066	153	0.031	518	0.047
35.0	25	0.017	160	0.032	368	0.034
54.0	4	0.009	72	0.015	133	0.012

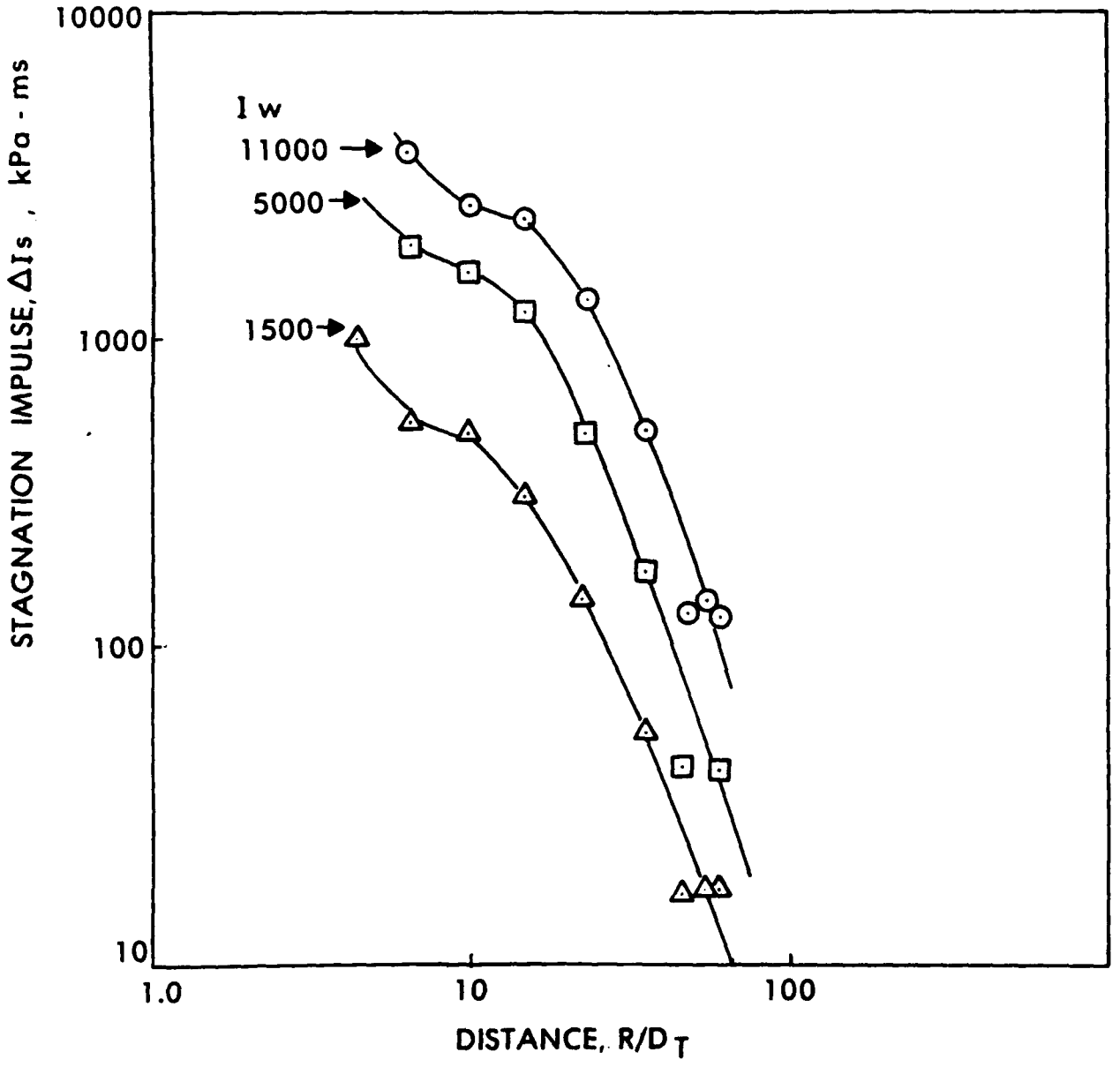

Figure 7. Stagnation impulse, (ΔI_s), versus range (R) over tunnel diameter (D_T) along the zero line for three pressure levels.

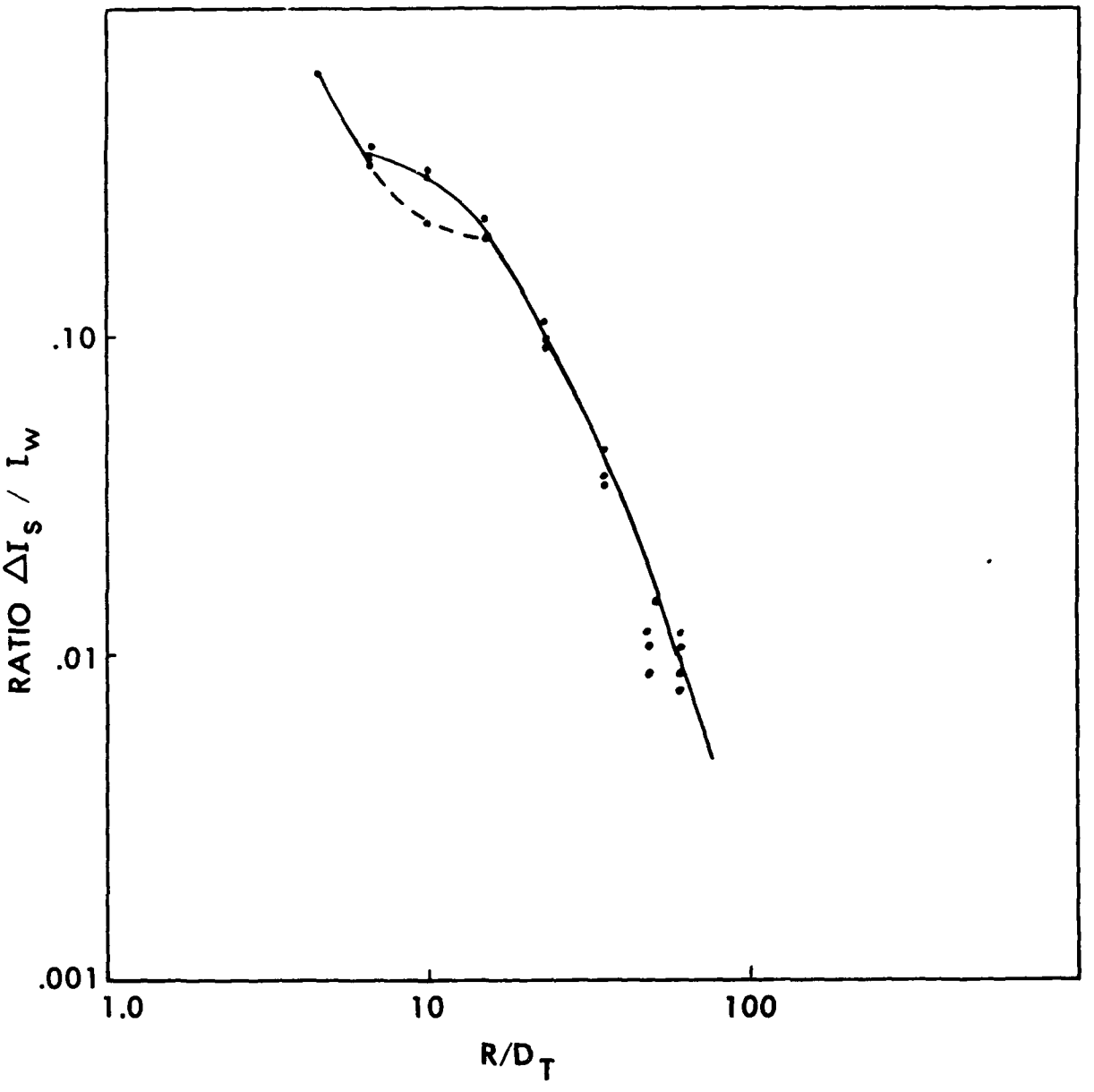

Figure 8. Ratio $\Delta I_s/I_w$ versus R/D_T.

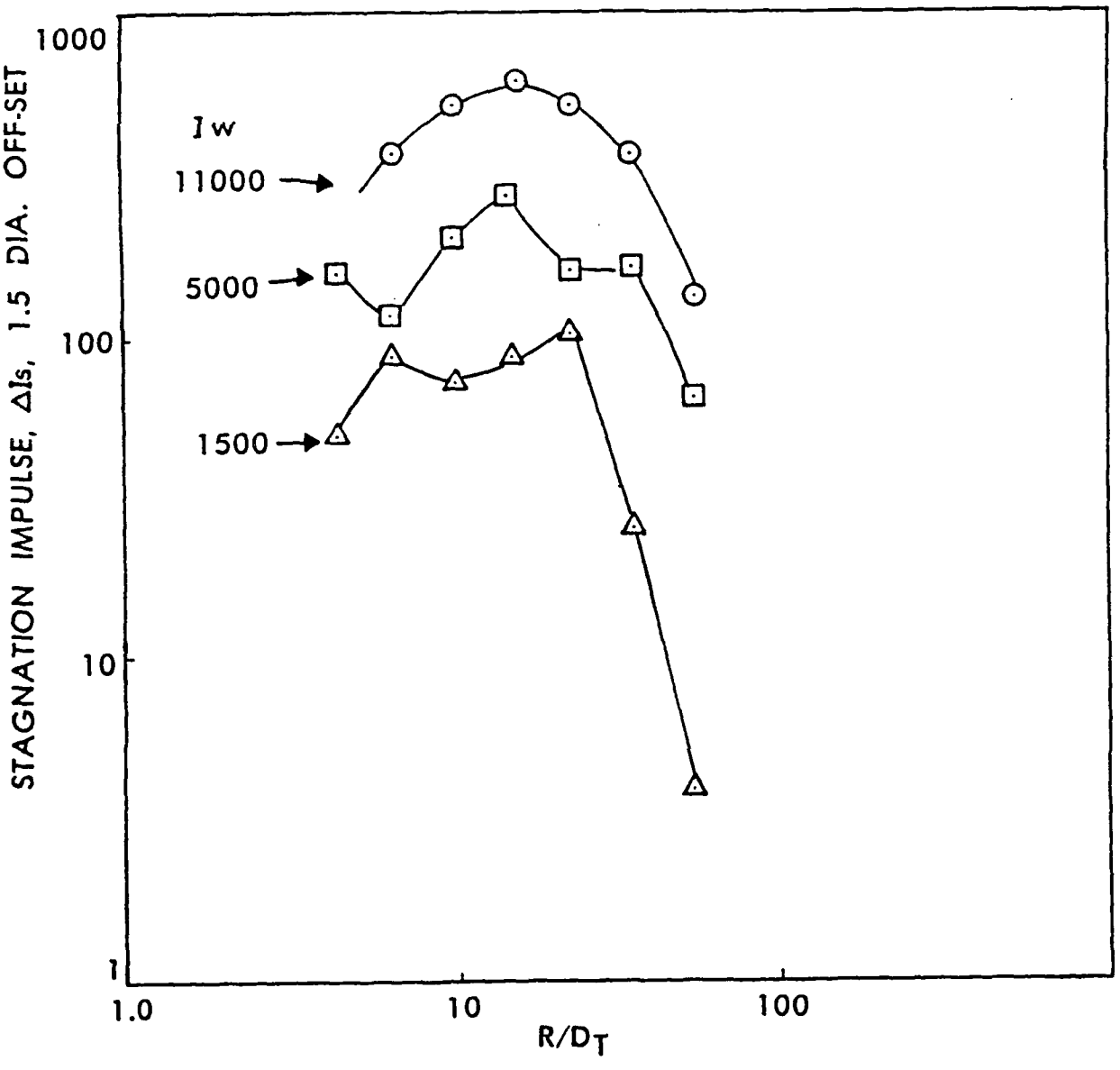

Figure 9. Stagnation impulse (ΔI_s) versus range (R) over tunnel diameter (D_T) along the 1.5-diameter line for three pressure levels.

3.2.3 Results along the 3.0-diameter line. The stagnation impulses measured along the 3.0-diameter line are listed in Table 3. These values are plotted in Figure 10. The 3.0-diameter line, when compared to the zero line, shows even a greater attenuation of stagnation impulse. If we look at station 10, we can see that, for the low pressure shots, the values are 479 kPa-ms for the zero line, 72 kPa-ms for the 1.5-diameter line, and 20 kPa-ms for the 3.0-diameter line. This shows that, with an offset of only three diameters, the stagnation impulse is only four percent of the zero-line values. These differences become even greater as we approach the tunnel exit.

3.3 Cube displacement measurements. In an effort to precisely map the jet-flow without establishing more blast lines, it was suggested that small cubes of different density material be used in place of stagnation probes. As shown in Equation 2, if the stagnation impulse and displacement are known, the constant, k, can be determined, and the cube can be considered calibrated. Now, if the cubes are placed at offset locations of 4, 5, 6, 7, 8, 9, or 10 diameters from the measured displacement, the stagnation impulse can be calculated.

3.3.1 Cube calibration. Cubes of two different sizes and three different materials were manufactured. They were steel, aluminum, and wood, sized one-inch and three-eighths-inch. The average weight of the three-eighths-inch steel cubes was 6.639 g; aluminum was 2.371 g; and wood was 0.5563 g. The one-inch steel cubes weighed 125.9 g; the aluminum was 45.0 g and the wood was 10.5 g. After the stagnation pressure versus distance was established along the zero line, then the cubes were placed at selected distances along the zero line, the shock tube was fired, and the displacements were measured. Care was taken to see that the cubes did not interfere with each other and that measurable displacements were obtained. From the blast line stagnation impulse, ΔI_s, at a specific distance, and the cube displacement, D, from that location, a relationship was established where $k = \Delta I_s/\sqrt{D}$. Because of the smallness of the shock tube and the sharp drop in ΔI_s values from the zero line to the three-diameter offset, the three-eighths-inch cubes were used for most of the offset measurements. A value of

$$k = .0202 \frac{\text{psi-s}}{\text{ft.}^{1/2}} \quad \text{or } 0.252 \frac{\text{kPa-s}}{\text{m}^{1/2}}$$

was established for the three-eighths-inch steel cubes, and

$$k = .006' \frac{\text{psi-s}}{\text{ft.}^{1/2}} \quad \text{or} \quad .076 \frac{\text{kPa-s}}{\text{m}^{1/2}}$$

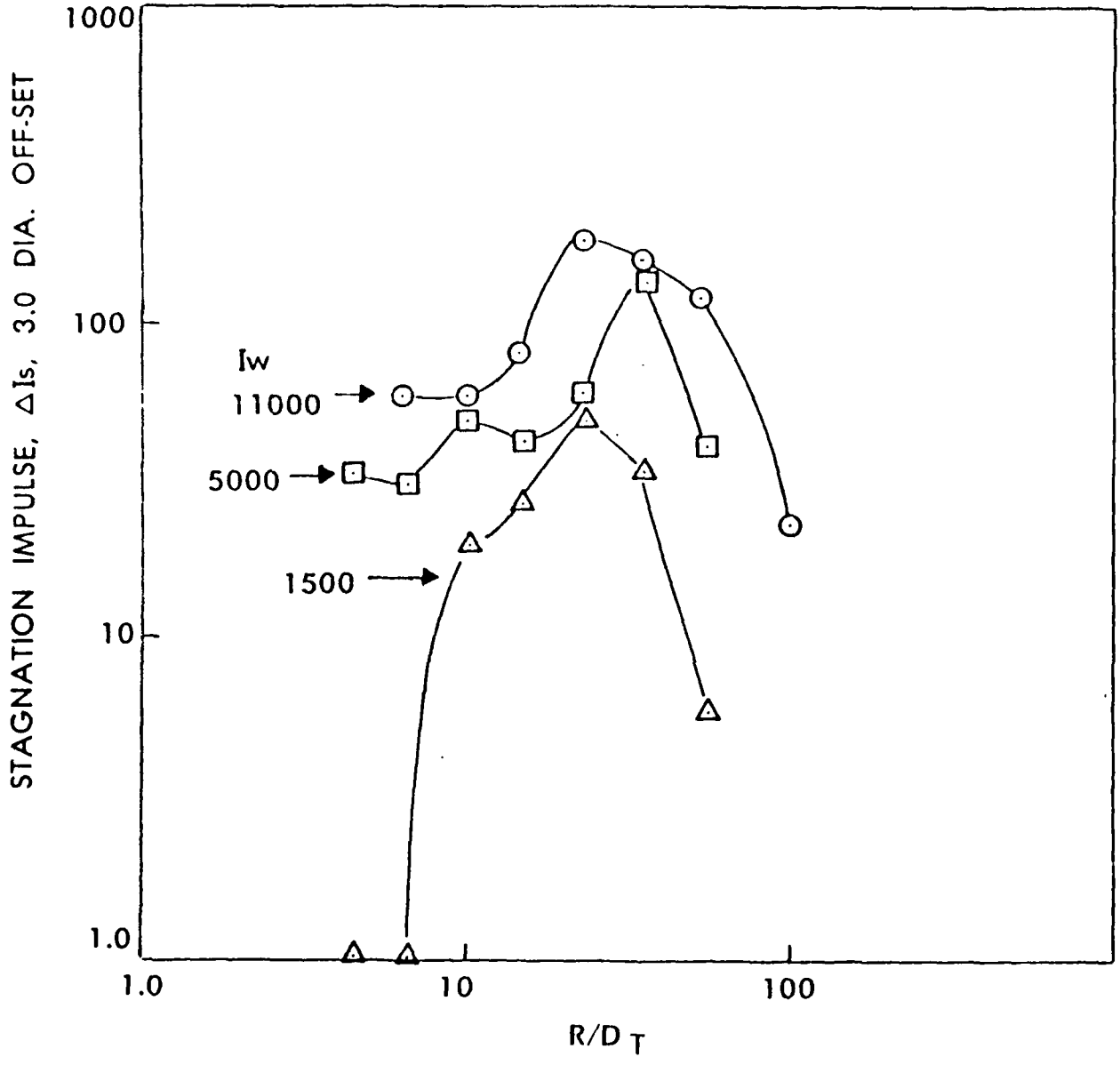

Figure 10. Stagnation impulse (ΔI_s), versus range (R) over tunnel diameter (D_T) along the 3.0-diameter line for three pressure levels.

TABLE 3. Stagnation Impulse along the 3.0-Diameter Offset Line.

Dist.	I_w=1,500	kPa-ms	I_w=5,000	kPa-ms	I_w=11,000	kPa-ms
R/D_T	ΔI_s kPa-ms	$\Delta I_s/I_w$	ΔI_s kPa-ms	$\Delta I_s/I_w$	ΔI_s kPa-ms	$\Delta I_s/I_w$
4.5	1	0.0006	34	0.0067	...	...
6.5	1	0.0006	31	0.0062	62	0.0056
10.0	20	0.0133	50	0.0099	60	0.0054
15.0	27	0.0180	44	0.0088	85	0.0074
23.0	50	0.0335	63	0.0103	188	0.0177
35.0	34	0.0227	131	0.0262	158	0.0144
54.0	5	0.0031	41	0.0082	123	0.0115
100.0	...	...	...	...	23	0.0020

TABLE 4. Stagnation Impulse Versus Offset for I_w = 1,500 kPa-ms, Cube Data.

	Impulse, kPa-ms						
Distance along zero line, dia.	Offset diameters 0	1.5	3.0	4.0	5.0	6.0	7.0
12	400	95	22	9.5	...	...	...
18	220	115	67	40	26	17	11
24	142	87	55	40	29	22	16
30	75	55	41	34	28	23	19
36	52	38	28	23	19	15	13
44	38	32	27	24	22	20	17
54	17	15	13	...	...	...	...

was established for the three-eighths-inch aluminum cubes. The constant, k, can be substituted in Equation 2 to determine the stagnation impulse at the offset position.

3.3.2 Cube impulse measurements. The stagnation impulse values based on cube displacements for various offset distances are listed in Table 4. Note that the distances along the zero line are different from those in Table 3 because a grid was established consisting of 0.3048 metre squares (one-foot squares) to assist in measuring displacement distances. From the cube displacements the impulses were calculated for various offsets at selected distances in front of the tube for specific exit conditions. The cube displacements were determined for the 1,500-kPa-ms exit impulse. When the offset impulses ΔI_s for a given distance in front of the tube was plotted on semi-log paper as ΔI_s versus offset, they fell along a straight line, which means that the decay from the zero line outward is exponential. At the close-in station, the slope is very steep, but it becomes less steep as the distance in front of the tube increases. An illustration of this trend is shown in Figure 11, where the data for 12, 24, and 36 diameters in front of the tube are plotted as ΔI_s versus offset.

3.4 Side-on and stagnation peak overpressure. The present quantity-distance criteria for the location of buildings, roads, and houses is based on the peak side-on overpressure expected from the accidental explosion of a high explosive. It is the purpose of this section to point out the magnitude of the stagnation overpressure developed along the zero-, the 1.5- and the 3.0-diameter lines because of the jet-flow emanating from the tunnel. The measured values of the side-on peak pressure along the zero line and the stagnation pressure along the zero-, the 1.5-, and the 3.0-diameter offset lines are listed in Table 5 for three different exit pressure levels. The values of side-on and stagnation pressure listed in Table 5 along the zero line have been plotted in Figures 12, 13, and 14 to make comparisons at the exit pressures of 503, 1,000, and 1,896 kPa.

For directly applicable comparisons of side-on and stagnation pressure, three side-on pressure levels were selected. These are 24.1 kPa (3.5 psi) at the unbarricaded intraline distance, 15.9 kPa (2.3 psi) the public traffic route distance, and 8.3 kPa (1.2 psi) the inhabited building distance. These values are listed in Table 6 with a ratio of stagnation pressure-side-on pressure to show the magnitude of the stagnation pressure when compared with the side-on pressure. The average magnitude of stagnation versus side-on pressure is 7.3 times at the intraline distance, 6.1 times at the public traffic route distance, and 4.0 at the inhabited building distance.

These ratios are significant and should be of concern in establishing any new quantity-distance criteria. The magnitudes of the stagnation pressure shown are along the zero line, but in Table 5 it can be seen that the effect, although not as great, is still evident at the 3.0-diameter offset line.

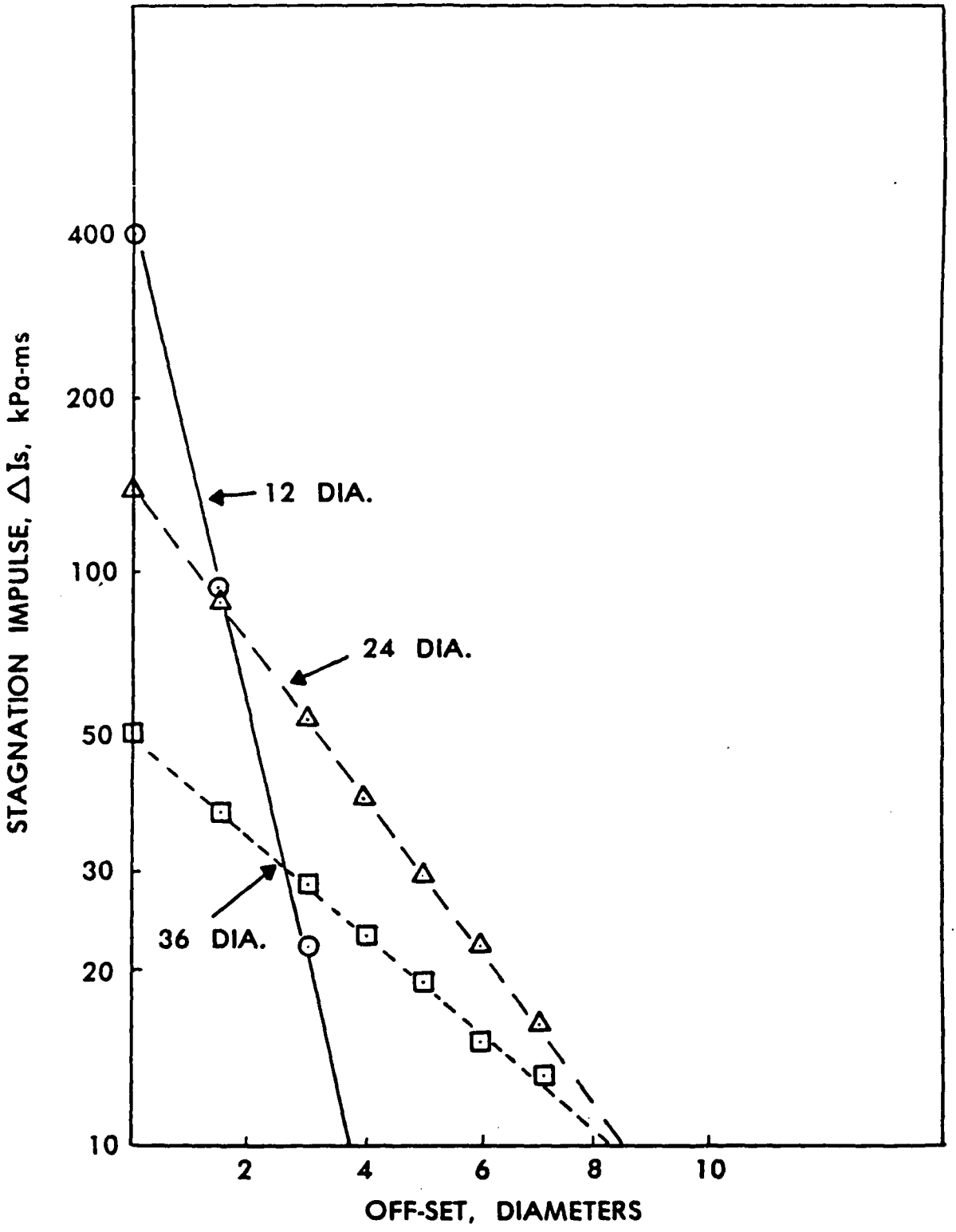

Figure 11. Stagnation impulse versus off-set for I_w = 1500 kPa-ms.

TABLE 5. Side-on and Stagnation Peak Overpressure.

Offsets	0		1.5	3.0	
Distance, dia	ΔP, kPa	P_{stag}, kPa	P_{stag}, kPa	P_{stag}, kPa	P_w, kPa
10	27.6	225.5	96.5	34.5	503
15	15.9	100.0	75.8	20.7	"
23	9.0	50.3	68.9	20.7	"
35	4.8	10.3	18.6	10.3	"
10	55.2	303.3	137.9	75.8	1, 000
15	31.7	200.0	103.4	34.5	"
23	17.9	151.7	137.9	41.4	"
35	10.3	48.3	48.3	34.5	"
54	6.2	11.7	11.7	11.7	"
10	101.4	379.2	303.4	186.2	1, 896
15	59.3	400.0	372.3	103.4	"
23	33.1	296.5	200.0	151.7	"
35	18.6	103.4	103.4	62.1	"
54	11.0	50.3	27.6	27.6	"

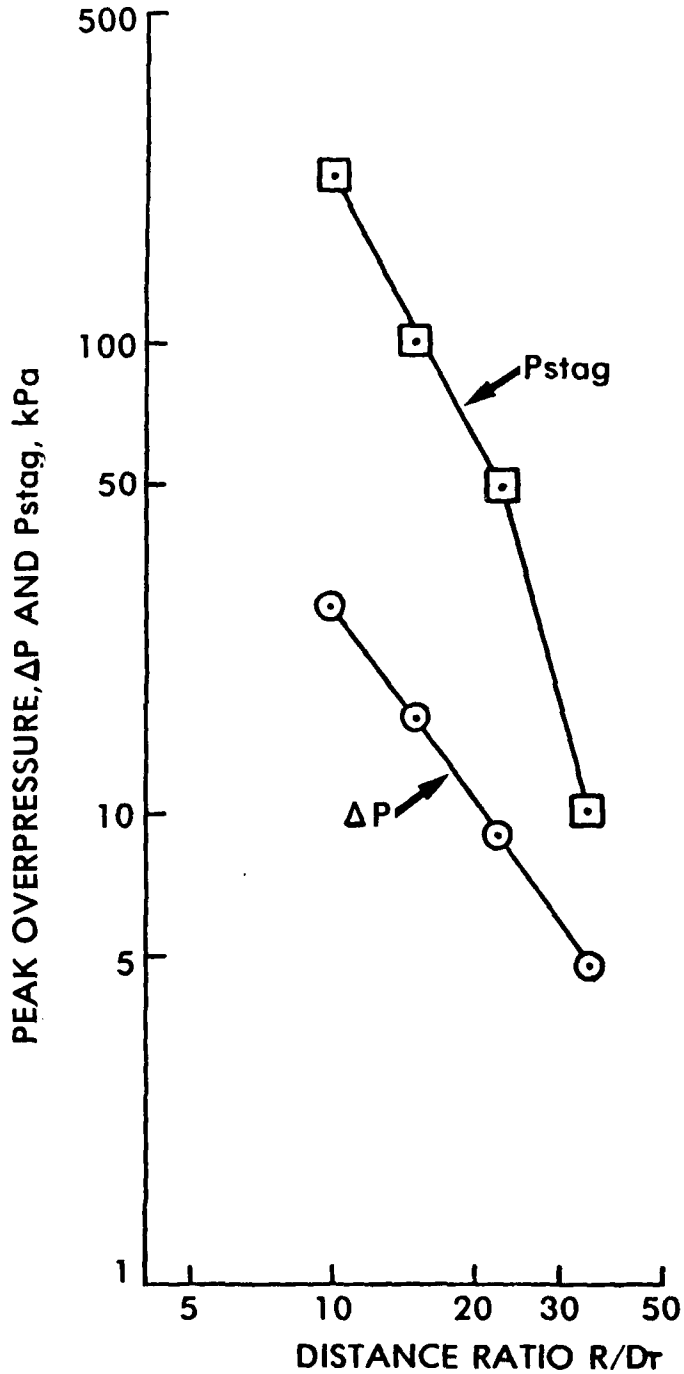

Figure 12. Side-on and stagnation pressure versus R/D_T for exit pressure of 503 kPa.

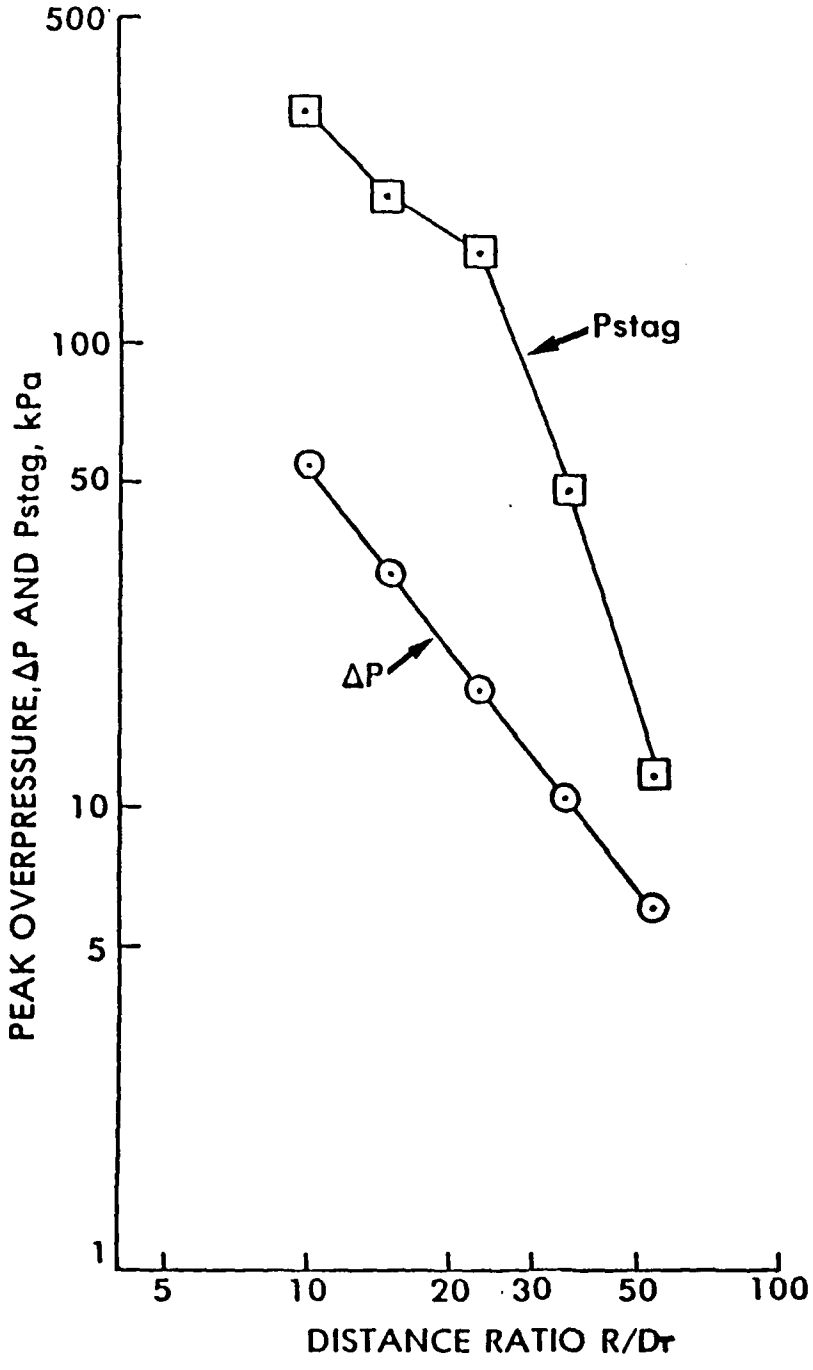

Figure 13. Side-on and stagnation pressure versus R/D_T for exit pressure of 1,000 kPa.

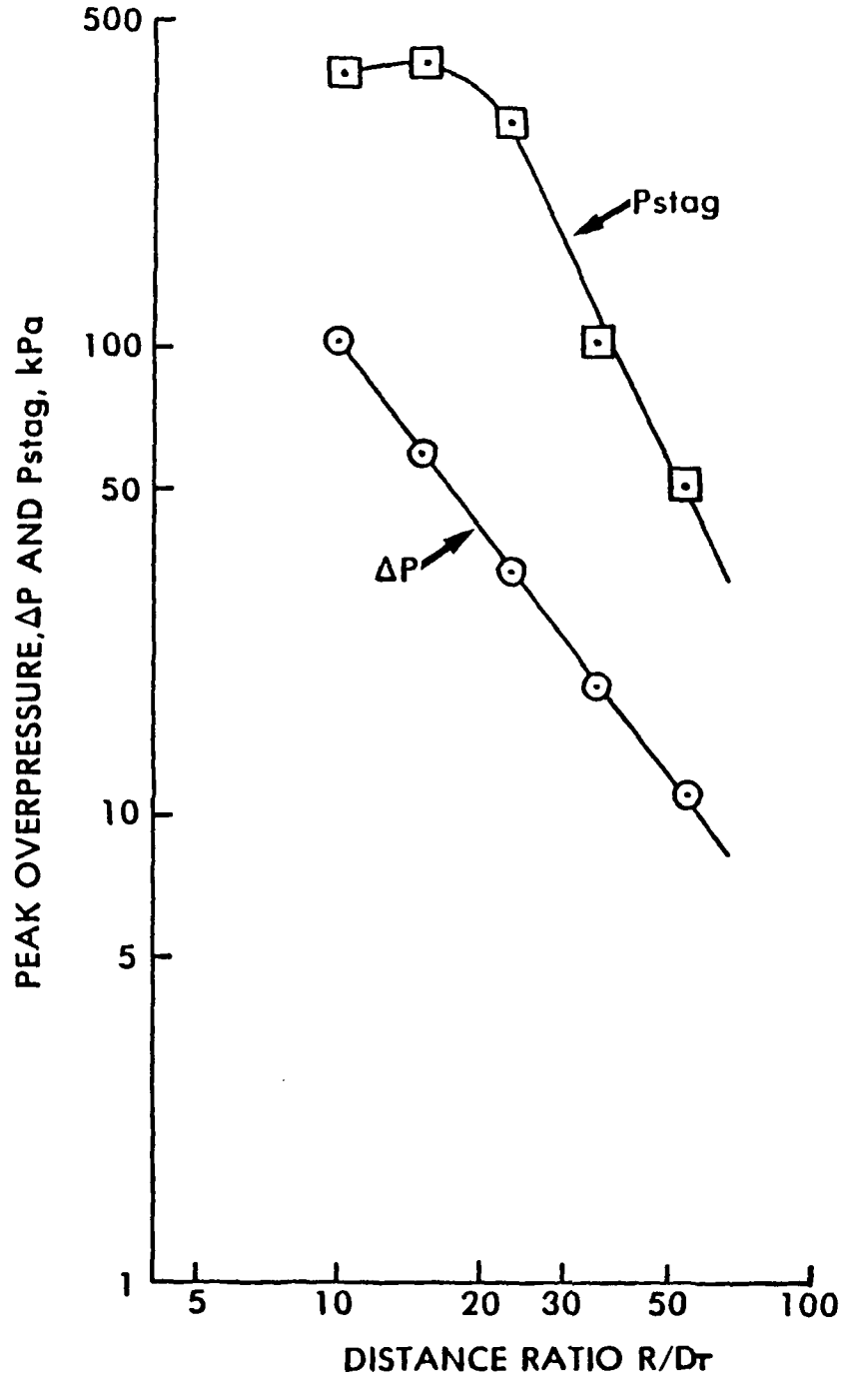

Figure 14. Side-on and stagnation pressure versus R/D_T for exit pressure of 1,896 kPa.

TABLE 6. Side-on Pressure versus Stagnation Pressure along the Zero-Degree Line.

Distance R/D_T	Exit pressure P_w, kPa	Side-on ΔP, kPa	Stagnation P_{STAG}, kPa	Ratio $P_{STAG}/\Delta P$
11	503	24.1	179.3	7.4
15	"	15.9	100.0	6.3
24	"	8.3	38.6	4.7
19	1, 000	24.1	172.4	7.2
26	"	15.9	100.0	6.3
42	"	8.3	27.6	3.3
29	1, 896	24.1	172.4	7.2
40	"	15.9	89.6	5.6
65	"	8.3	33.1	4.0

4. CONCLUSIONS

4.1 Magnitude and extent of jet-flow. Based on the transducer measurements, and cube displacements, it can be concluded that the jet-flow exiting from the shock tube is high velocity, very turbulent, relatively narrow, and can add significantly to target loading. The magnitude, in terms of stagnation impulse, is a function of the exit energy or side-on impulse, offset from the zero radial, and distance from the exit. The magnitude, in terms of peak stagnation pressure, is a function of the exit pressure, offset from the zero radial, and distance from the exit. These conclusions are based on the jet-flow documented from a 2.54-cm-diameter shock tube with a helium driver. At this time there are indications from recent tests using high explosives in scaled munition storage models that a high velocity flow does exist along the zero radial but the magnitude has not been quantified.

Table 5 shows that the stagnation pressure drops rapidly with offset, and beyond 5 diameters offset, there is little effect from the jet.

4.2 Shadowgraph documentation of the jet-flow. After the bulk of the report was completed, a small program was initiated to determine whether the jet-flow could be documented with a shadowgraph technique. The results of this work are presented in Appendix B.

Some conclusions based on the shadowgraph pictures are that the shockwave moves out far ahead of the jet. At the lower exit pressure, ~ 500 kPa, the jet velocity at 7.5 diameters is 254 m/s but decreases to 66 m/s at 37 diameters. The jet-flow is very turbulent and is not always symmetrical about the zero line.

REFERENCES

1. Kingery, Charles N., Survey of Airblast Data Related to Underground Munition Storage Sites, BRL Technical Report to be published.

2. Ammunition and Explosives Safety Standards, DOD Manual 6055.9-STD, July 1984.

3. James, D. J., An Investigation of the Pressure Waves Propagated from the Opened End of a 30" x 18" Shock Tube, AWRE Report 0-60/65, AWRE, England, September 1965.

4. Ethridge, N. H., Use of Displacements of Cubes as a Measure of Blast, Unpublished report, Aberdeen Research Center, Aberdeen, MD., _____ 1987.

5. Schmidt, E. M. and Shear, D. D., The Flow Field about the Muzzle of an M-16 Rifle, BRL R1692, January 1974.

APPENDIX A

Sample Pressure Traces for Shock Tube Jet-Flow

APPENDIX A

Some sample traces are shown in this appendix that were unavailable at the time the report was written. The traces will illustrate some of the waveforms and the features discussed in the text.

Figure A-1a shows the exit side-on overpressure and associated impulse for our lowest level shock and driver overpressure, and Figure A-1b shows the exit stagnation overpressure and impulse for this level. Figure A-1c shows the exit side-on overpressure and impulse for an intermediate level shot. This is a typical level appropriate for the following series of traces that depict the flow characteristics at distances beyond the "tunnel" exit. The exit side-on pressure waveform, following the more-or-less ragged rise to the peak indicating the shock passage--will exhibit noticeable "flattening" (depending on exit flow speed and Mach number) because the exit flow becomes sonic due to the interactions there. This is followed by the steep decay due to the closed-end reflected rarefaction wave arriving at the exit, then the gradual decay to ambient. It was of interest to note that the tube's air shock exited supersonically at all three of our shock pressure levels. However, the helium jet exited subsonically at the lowest shock level, near sonic at the intermediate level, and supersonically at our highest shock level.

Figure A-2a shows an example of pressures along the zero-degree line, at the approximate 3-4, 2, and 1 psi levels of DDESB interest. It illustrates the side-on pressure behavior with distance downrange from the exit. The corresponding stagnation pressures for the stations are shown in Figure A-2b. Note the enhanced levels due to the jet-flow over stations 23 and 35. At station 54 the jet-flow enhancement is essentially gone, but the flow-positive duration and, hence, the loadings on a target, have increased.

The series of traces of Figures A-3 - A-5 show the jet-flow effects with offset from the centerline, at stations 10, 23 and 54, respectively. These are again at the mid-level exit pressure of our shots. The top trace is the side-on pressure, for reference. Then, in order down the page are stagnation pressure at zero-, 1.5-, and 3.0-diameter offset. Note the dramatic decrease of level at only 3.0-diameter offset over stations 10 and 23. Levels are pretty much that of the side-on levels. These results indicate that the jet-flow is quite narrow but also significant. At station 54 where the side-on level is below 10 kPa (1.5 psi), the jet-flow has apparently broadened, and levels are even from zero to 3.0 diameters. Some later tests were conducted to observe the jet-flow photographically. (See Appendix B.)

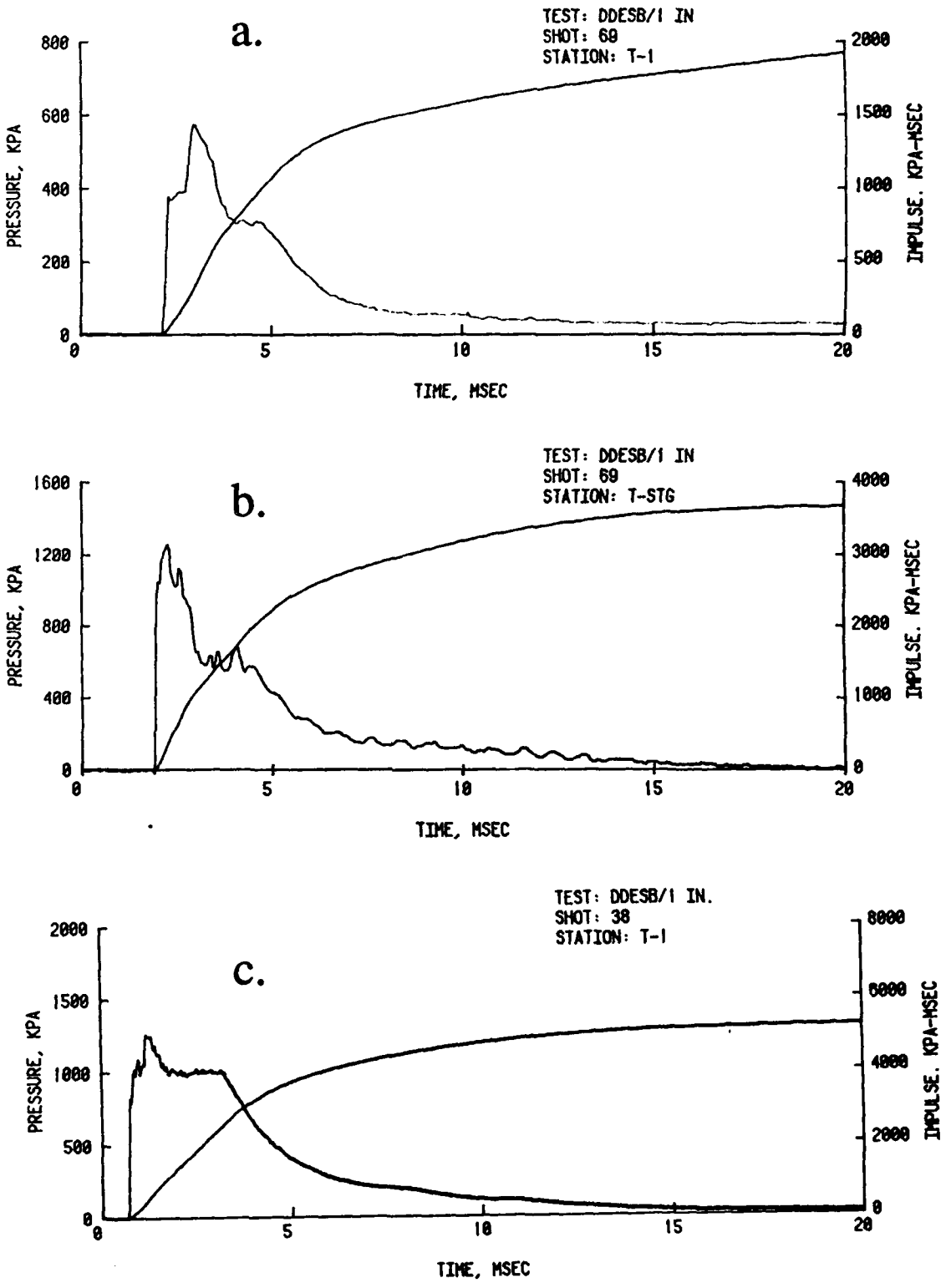

Figure A-1. Sample exit pressure traces for shock tube jet-flow.

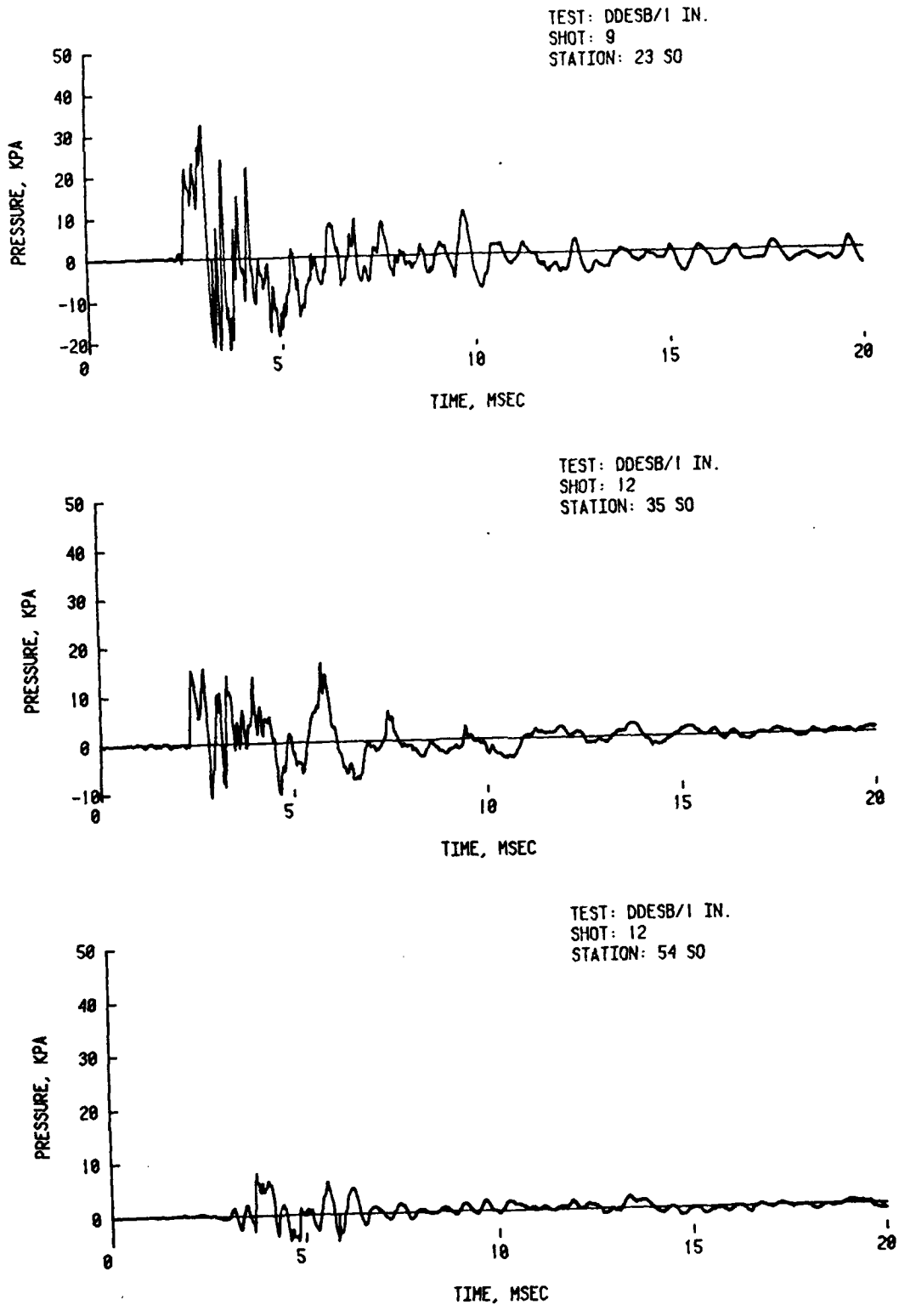

Figure A-2a. Side-on pressure levels at stations along zero line.

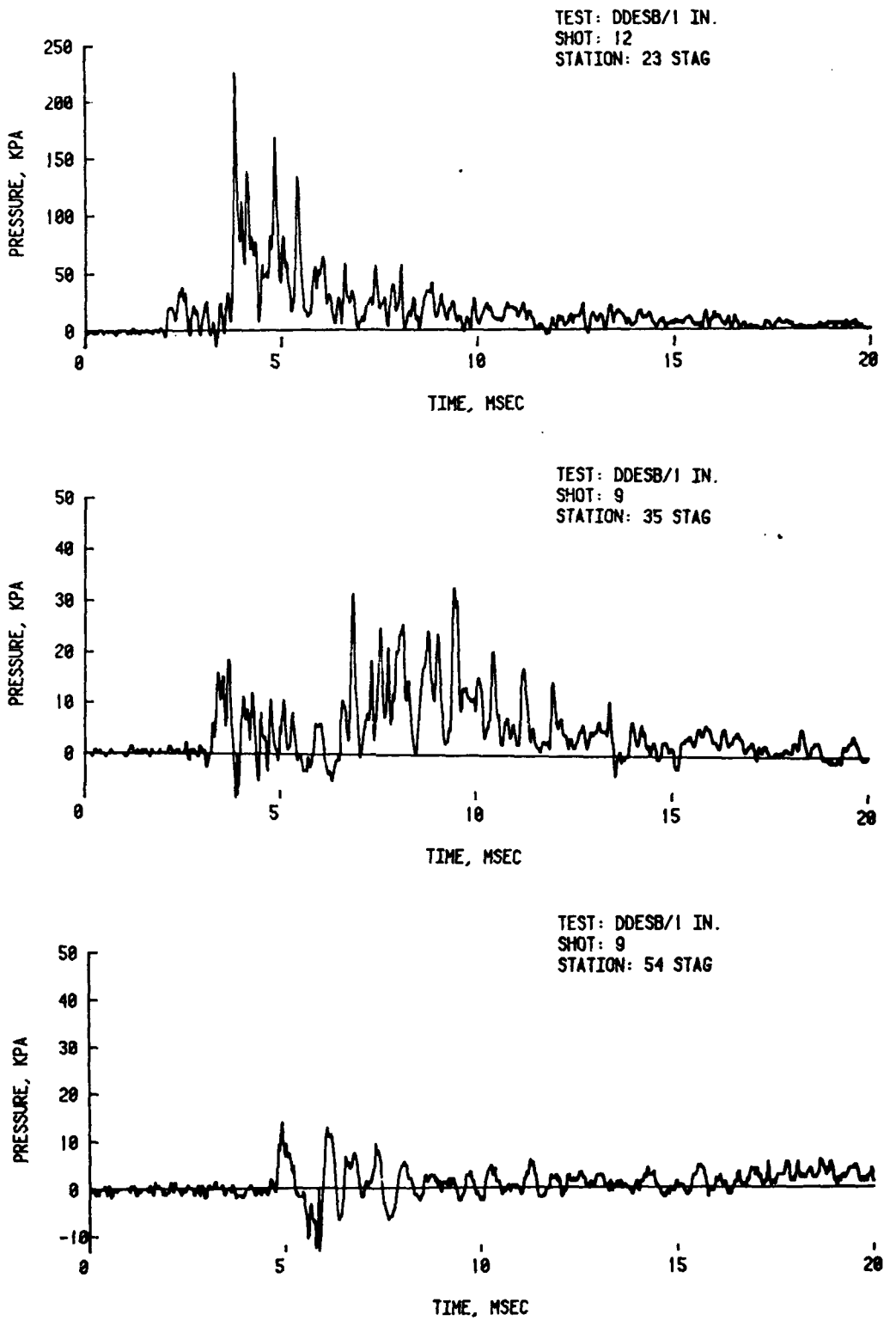

Figure A-2b. Stagnation pressure levels along zero line.

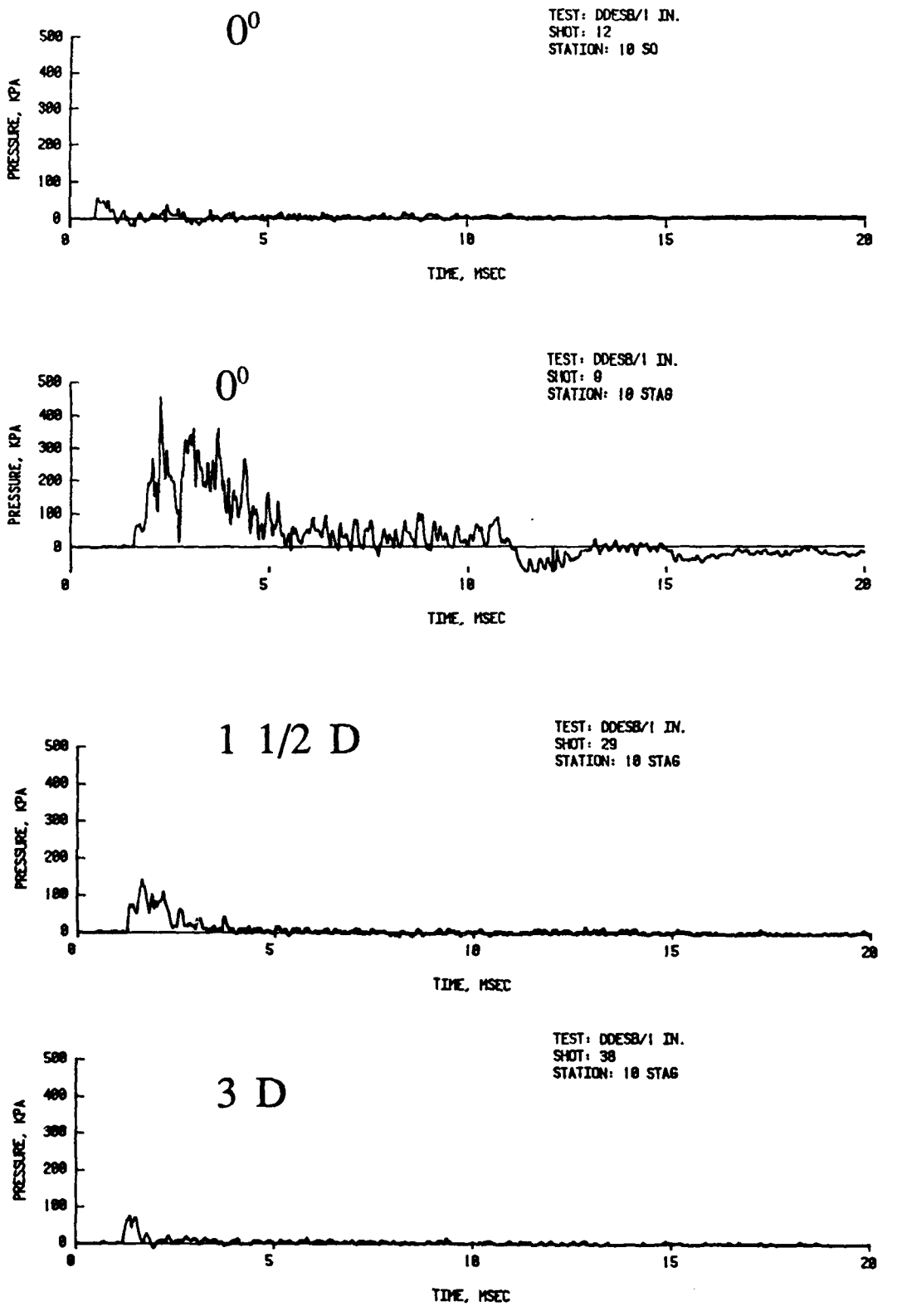

Figure A-3. Pressure levels at offset locations--10 D from exit.

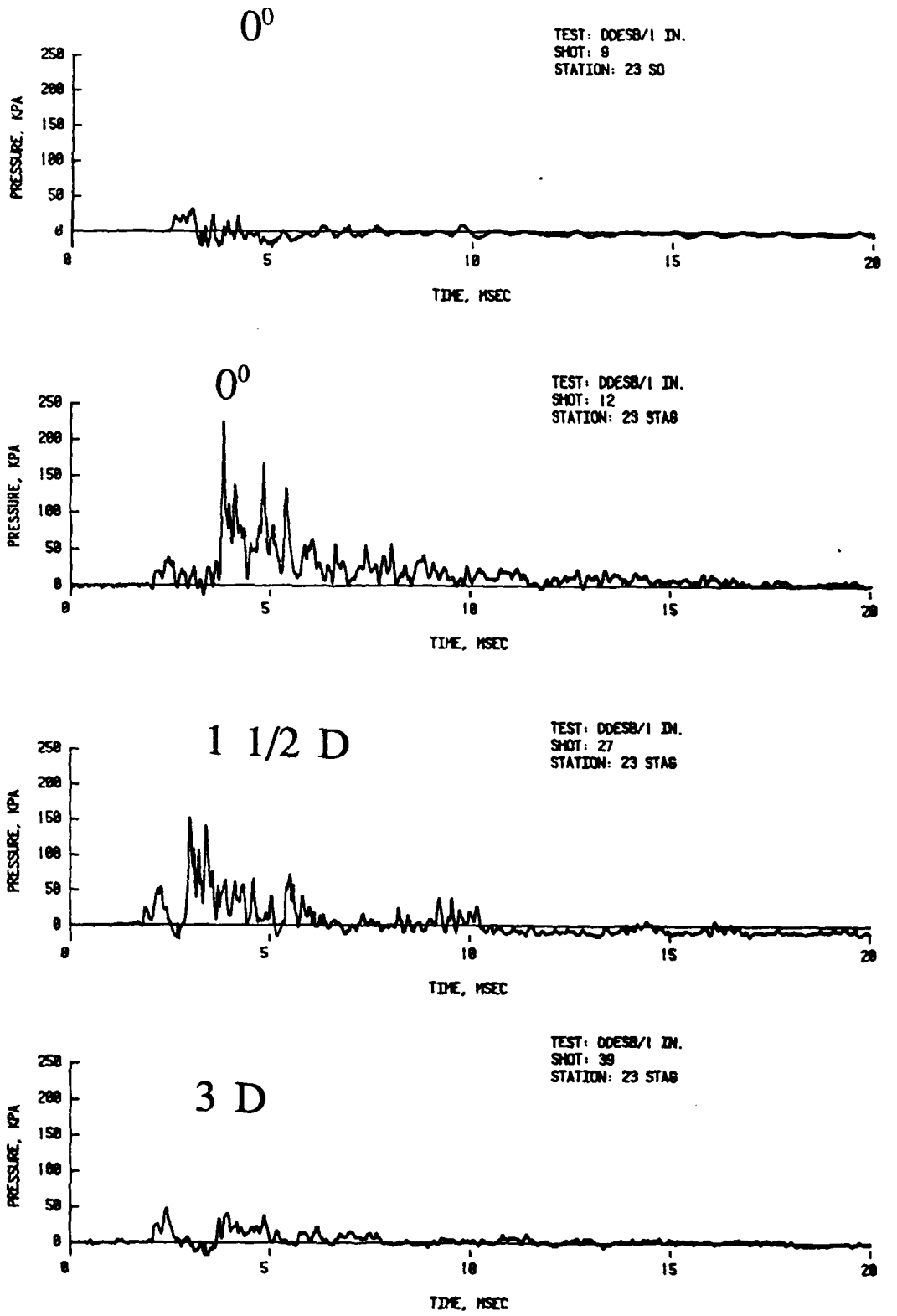

Figure A-4. Pressure levels at offset locations--23 D from exit.

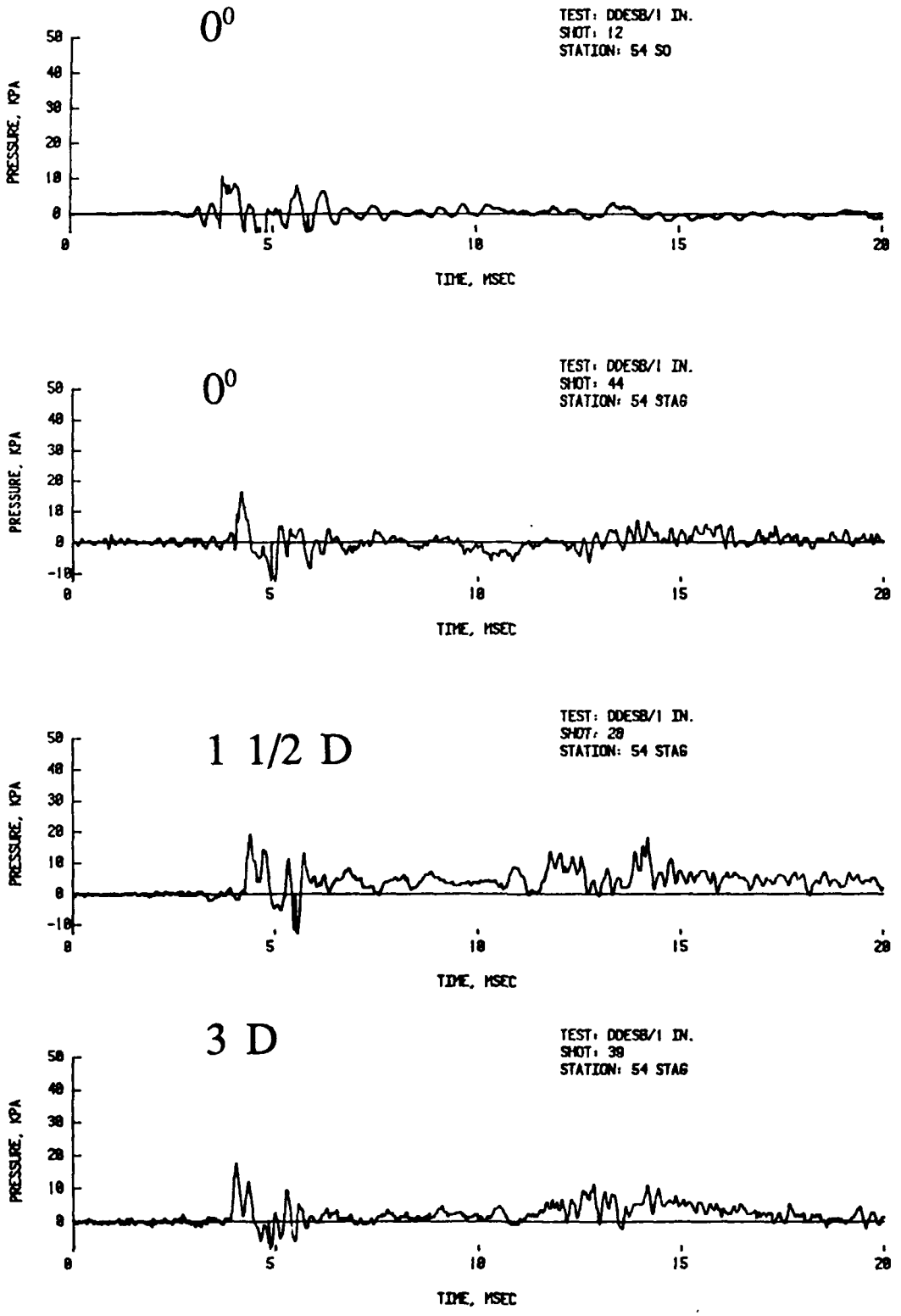

Figure A-5. Pressure levels at offset locations--54 D from exit.

APPENDIX B

Shadowgraphs of Shock Tube Jet-Flow

APPENDIX B

A limited number of shadowgraphs have been made to pictorially document the velocity and size of the jet-flow exiting the shock tube at the lower pressure level. These shadowgraphs should prove useful in delineating the jet-flow extent and should assist in corroborating the measurements by pressure gages and displacement cubes. The structure and characteristics of jets are objects of continuing study, due to their diverse applications. However, it appears that most of the information is confined to a region close to the jet exit. For our purposes here we have observed the region out to 40 exit diameters, where photographs of the jet-flow seem rather uncommon. We note the excellent shadowgraphs by Schmidt and Shear[5] of the muzzle-blast jet-flow to 50 diameters outward. However, muzzle jet exit pressures may range from 100-300 atm typically, some 20 to 30 times the levels used in this work. Thus, due to the exit mach number dependence of the jet-flow, features are not directly comparable.

Apparatus and Setup. Because of the small scale of the jet involved, a single spark source, a Hi Voltage Components, Inc., Model SS55P, was used. The unit was placed 1.09 m (42.5 in) above the ground plane/platform, which presented the most convenient geometry for the photography. The one source was deemed sufficient to illuminate approximately 24 diameters of the flow extent in enough detail for analysis. Additionally, it seemed appropriate to concentrate efforts on the lowest level flow, to be assured of adequate lighting and exposure. Setting up for the shadowgraphs involved elevating the shock tube to maintain a relative position with respect to the three 20 x 25-cm (8 x 10-in) film holders and the covering glass sheet, simulating a portion of the ground plane. The spark source with built-in power supply, triggered by an Orthometrics Type 308b time-delay unit, which receives the signal from the shock tube's exit pressure gage, constitutes the simple shadowgraph setup. Filmholders could be offset from the centerline position to cover the flow extent more fully. In Figure B-1 a sketch of the setup and location of the filmholders in relationship to the tube exit is shown.

Results. At a single condition corresponding to the lowest driver pressure, with exit pressure from 500-600 kPa, a number of shots were fired to give shadowgraphs at 1.5, 3.0, 4.0, 5.0 and 6.25 ms after shock exit. Some sample shadowgraphs are shown in Figure B-2. The 20 x 25-cm film negatives have been printed at a reduced size for inclusion in this report. In Figure B-2a the jet-flow is shown at a delay time of 3.0 ms on film position 2. The back edge of the film was 21.9 tube diameters from the tube exit. With the short delay times, filmholder 2 was centered along the tube axis or zero line.

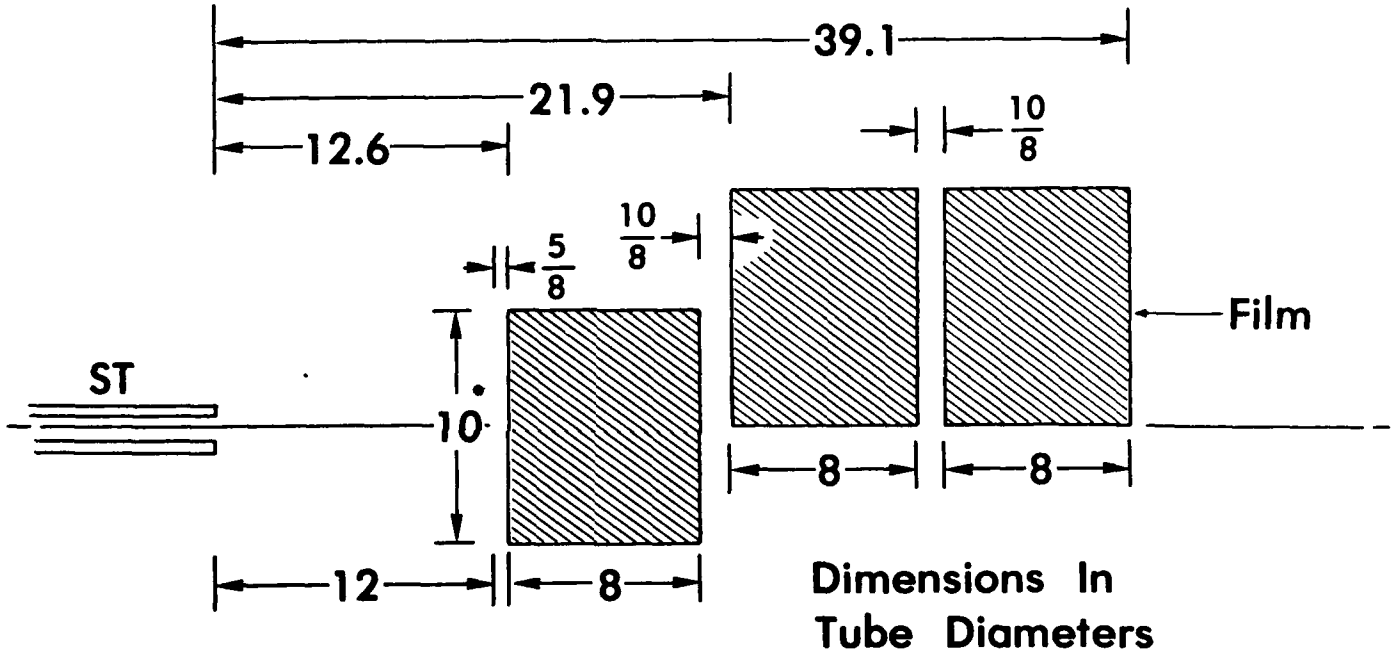

Figure B-1. Location of film.

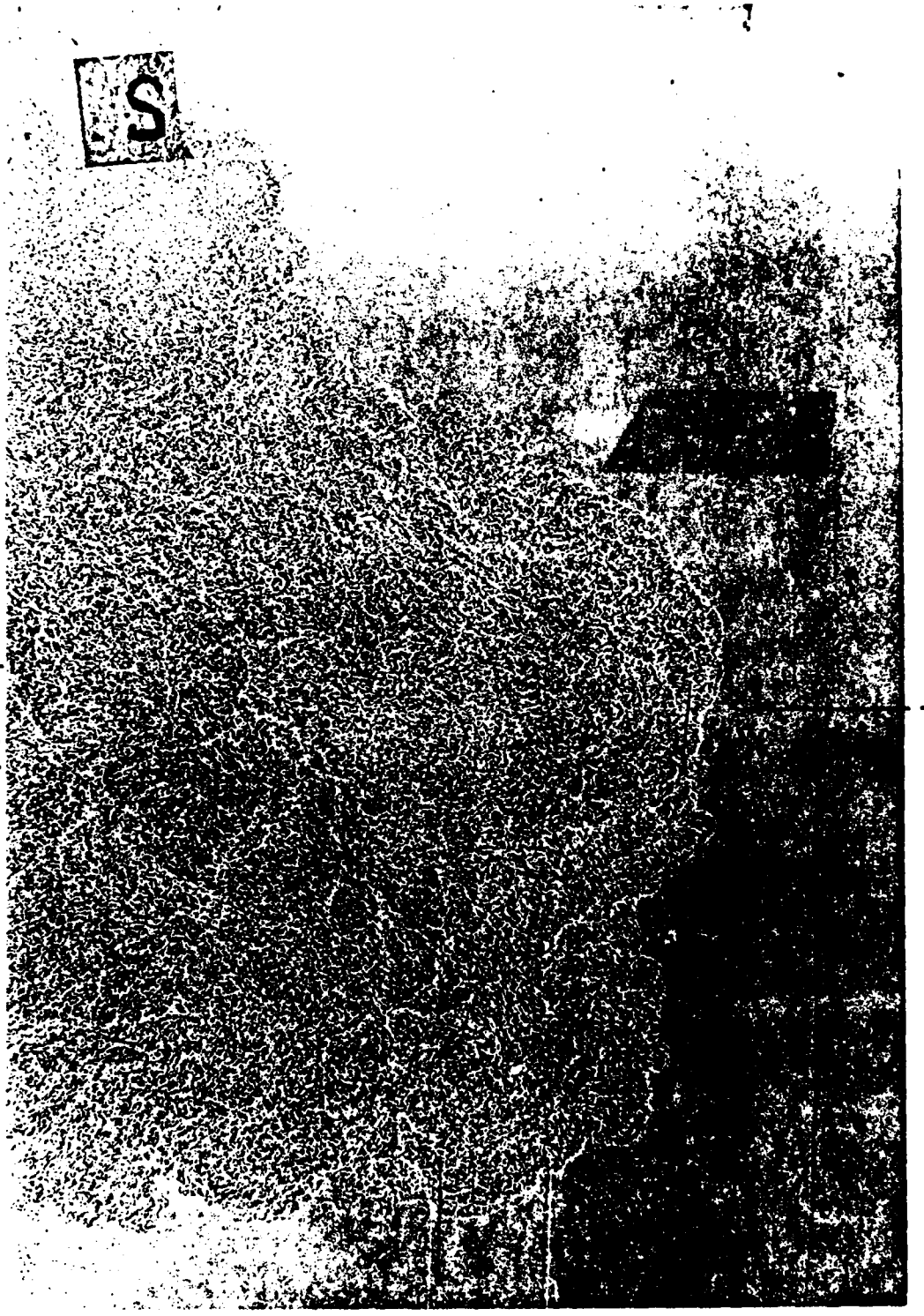

Figure B-2a. Shadowgraph of jet-flow at 3-ms delay time.

In Figure B-2b the jet is shown at a delay time of 4.0 ms where the filmholder has been offset with one film edge aligned with the zero line. The jet displays a greater forward expansion than lateral expansion.

In Figure B-2c the delay time is 6.25 ms, and the filmholder is 3 with the back edge located at 31.1 diameters. The jet velocity has decreased at this distance and also shows a considerable lateral expansion.

Tracings of the jet boundaries from reduced scale prints of the shadowgraph negatives are shown in Figure B-3, with distances shown from the tube end as well as laterally. The gaps between the traces, which have been connected with dotted lines, are due to the finite widths of the film holders along the actual film. Observation begins beyond 12 tube diameters since our interest was in the farther region of the jet. It is interesting to note the close-in behavior of the jet. At 1.5 ms after shock exit, the jet-flow has traveled to approximately 15 diameters but extends laterally to less than 4 diameters half-width. Also, the jet width exhibits an apparent pulsation in width with time.

Farther out, onto films 2 and 3, the jet width still maintains its narrow width to 4.0 ms, then diffuses laterally as the forward moving gases slow down and retard the advance of the following gas, forcing it to the side. It seems plausible to associate the significant loading effects of the jet-flow with the jet when it is narrow and concentrated, which is, according to the shadowgraphs, up to a distance of 28-30 diameters from the tube exit.

Such a picture is in agreement with the data of Table 5 for the Pw = 500 kPa level of the shadowgraph and for the corresponding curves at the scaled impulse for Iw = 1500 kPa-ms of Figures 7, 9, and 10. These figures give the stagnation pressure and impulse containing the jet contribution to loadings. One sees at the zero-, 1.5-, and 3.0-diameter offset lines significant loadings out beyond the 23-diameter station, but a sharp drop-off at the 35-diameter station. Thus, with the new shadowgraphs of the flow out to 40 diameters, we feel we have confirmed the narrow directivity and extent of the jet-flow and demonstrated the enhancement of loadings due the jet-flow.

The arrival times of the jet at measured distances for different delay times have been plotted in Figure B-4. From these data points a curve was established, and it was possible to calculate the average jet-front velocity between selected distances. These calculated average velocities are listed in Table B-1 where a dramatic decrease in velocity can be seen as the distance increases.

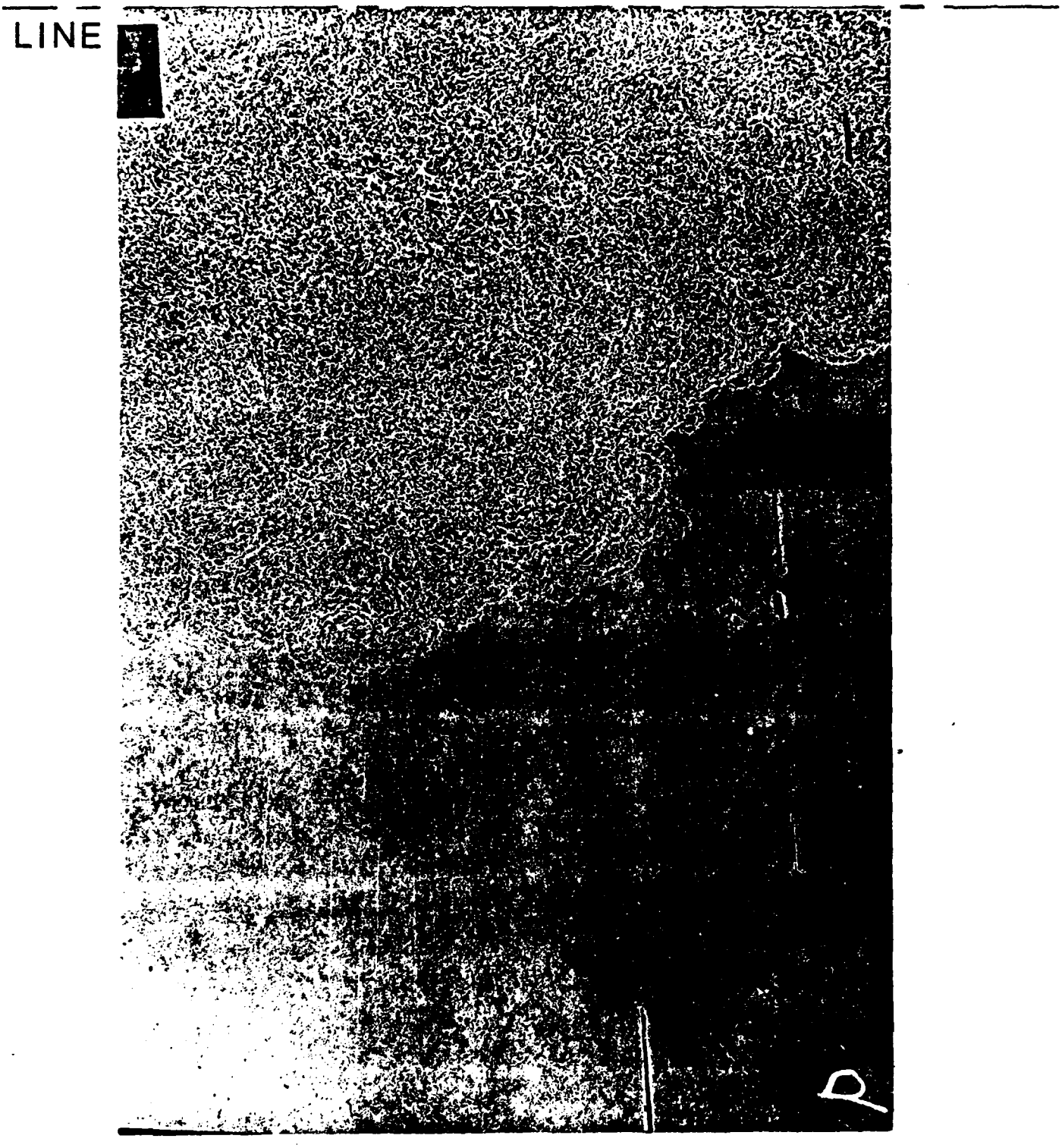

Figure B-2b. Shadowgraph of jet-flow at 4.0-ms delay time.

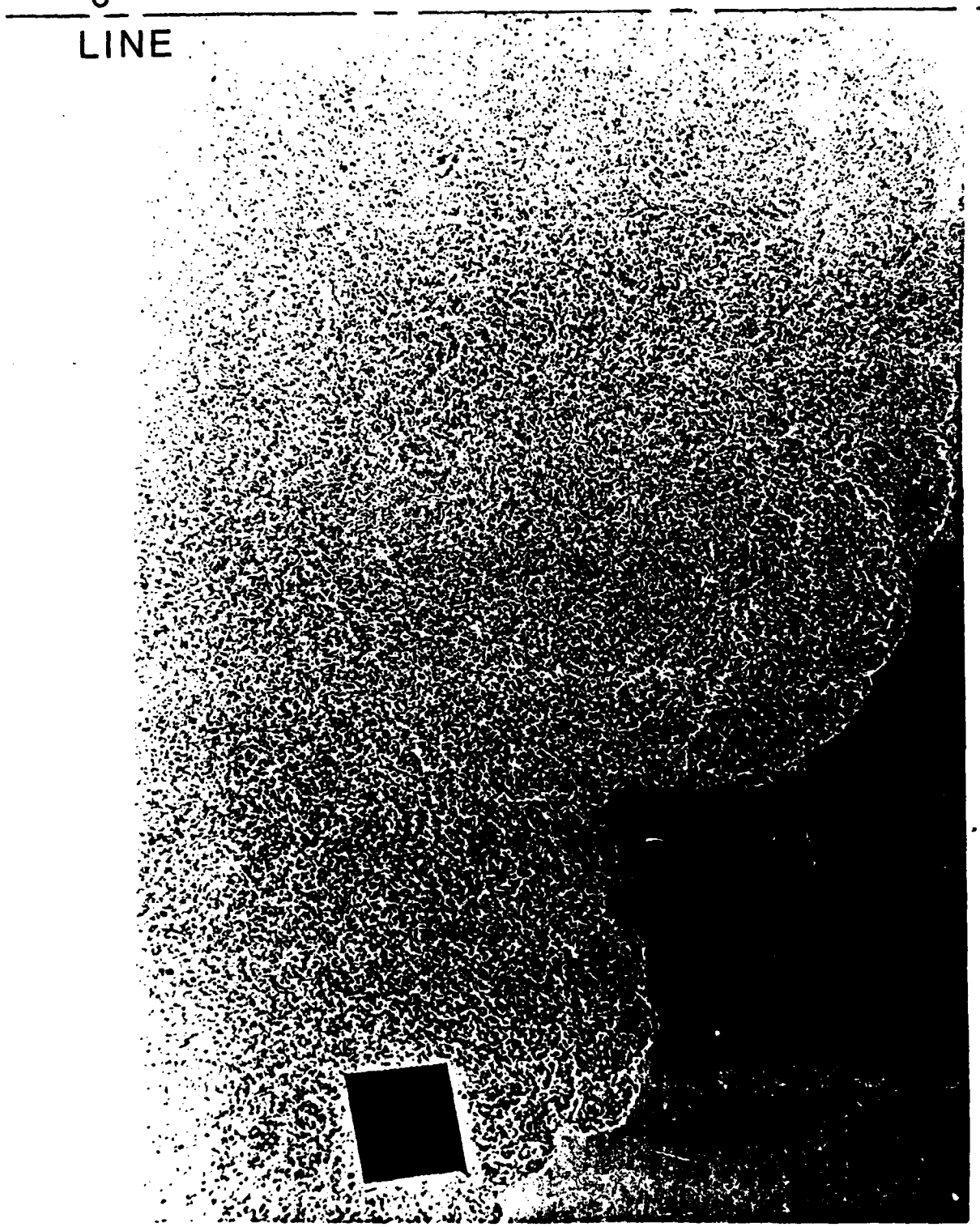

Figure B-2c. Shadowgraph of jet-flow at 6.25-ms delay time.

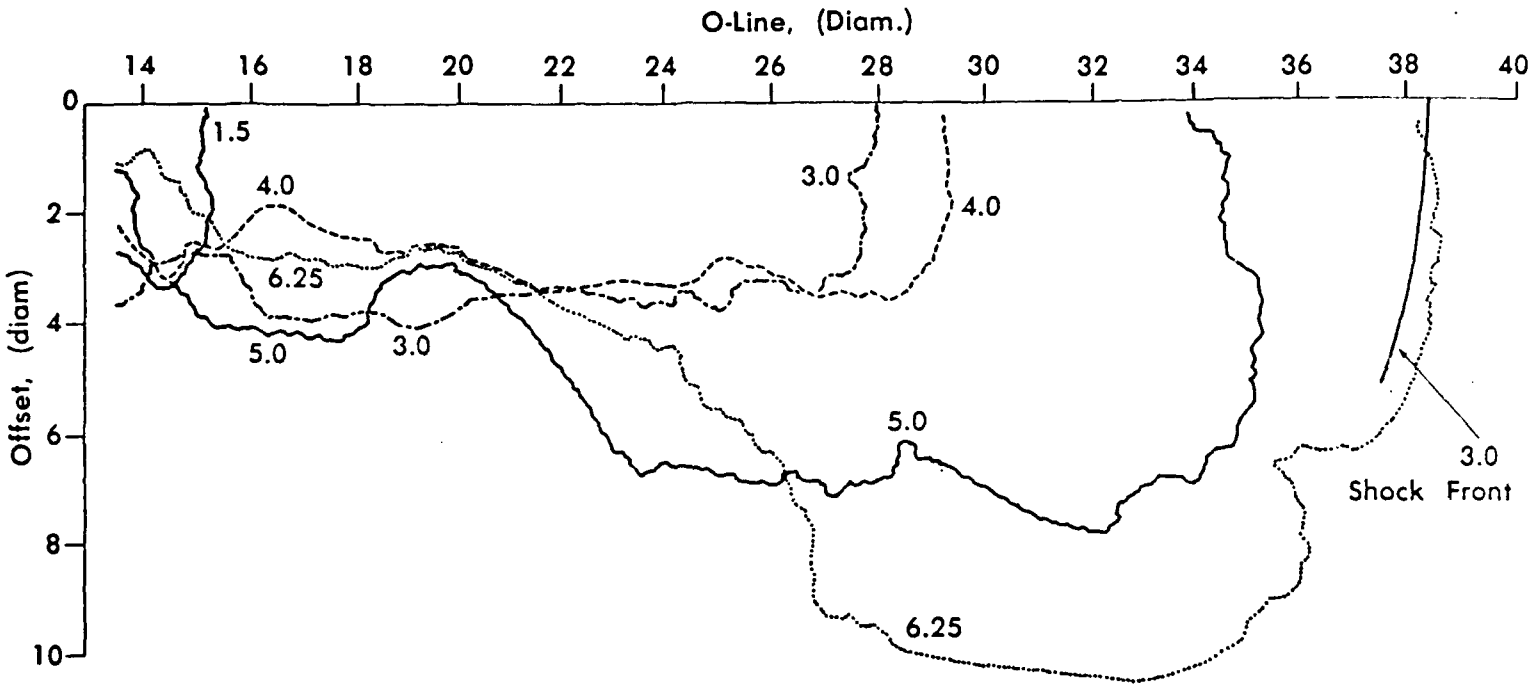

Figure B-3. Tracings of the jet boundaries at different delay times.

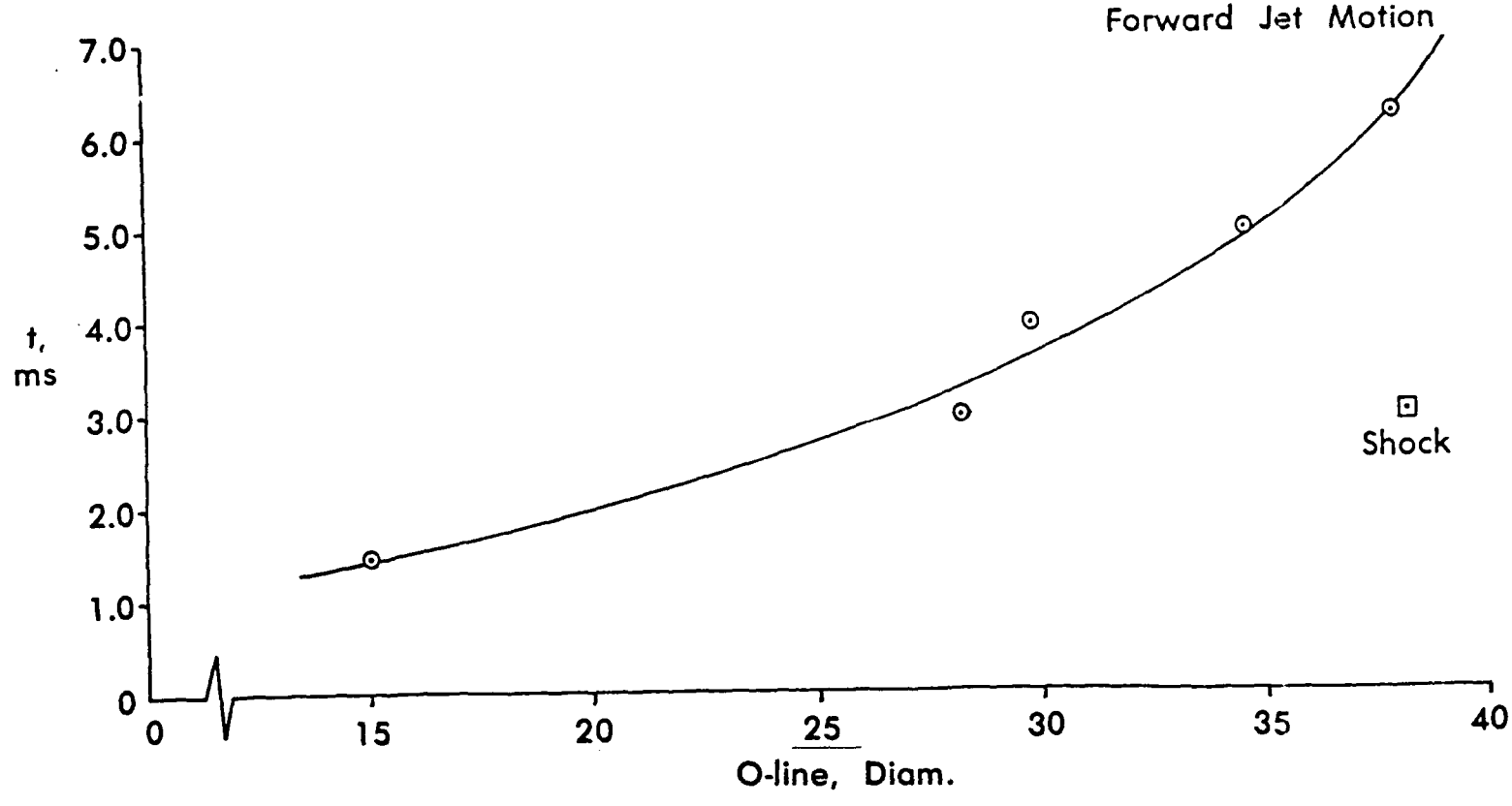

Figure B-4. Jet arrival time versus distance.

TABLE B-1. Average jet-front velocities.

Distance, diameters	Average Velocity, m/s	Mid-point, diameters
0 - 15	254	7.5
15 - 20	254	17.5
20 - 25	176	22.5
25 - 30	129	27.5
30 - 35	90	32.5
35 - 38	66	37.0

DISTRIBUTION LIST

No. of Copies	Organization
12	Administrator Defense Technical Info Center ATTN: DTIC-DDA Cameron Station Alexandria, VA 22304-6145
1	HQDA (SARD-TR) Washington, DC 20310-0001
1	Office Secretary of Defense ADUSDRE (R/AT) (ET) ATTN: Mr. J. Persh, Staff Specialist, Materials and Structures Washington, DC 20301
1	Under Secretary of Defense for Research and Engineering Department of Defense Washington, DC 20301
1	Director of Defense Research and Engineering Washington, DC 20301
1	Commander US Army Laboratory Command ATTN: AMSLC-DL Adelphi, MD 20783-1145
1	Director Benet Weapons Laboratory Armament RD&E Center US Army AMCCOM ATTN:SMCAR-LCB-TL Watervliet, NY 12189-4050
1	Commander US Army Armament, Munitions and Chemical Command ATTN: SMCAR-ESP-L Rock Island, IL 61299-5000
1	Commander US Army Aviation Systems Command ATTN: AMSAV-DACL 4300 Goodfellow Blvd. St. Louis, MO 63120-1798
1	Assistant Secretary of Defense (Atomic Energy) ATTN: Document Control Washington, DC 20301
1	Assistant Secretary of Defense (MRA&L) ATTN: EO&SP Washington, DC 20301
1	Director Defense Advanced Research Projects Agency 1400 Wilson Boulevard Arlington, VA 22209
1	Director Defense Intelligence Agency ATTN: DT-1B, [illegible] J.Vorona Washington, DC 20301
2	Chairman Joint Chiefs of Staff ATTN: J-3, Operations J-5, Plans & Policy (R&D Division) Washington, DC 20301
4	Director Defense Nuclear Agency ATTN: SPTD, Mr. T. E. Kennedy DDST (E), Dr. E. Sevin OALG, Mr. T. P. Jeffers LEEE, Mr. J. Eddy Washington, DC 20305

DISTRIBUTION LIST

No. of Copies	Organization
1	Commander Field Command Defense Nuclear Agency ATTN: Tech Lib, FCWS-SC Kirtland AFB, NM 87115
30	Chairman Department of Defense Explosives Safety Board 2461 Eisenhower Avenue Alexandria, VA 22331
1	HQDA (DAMA-ART-M) Washington, DC 20310
1	HQDA (DAEN-ECE-T/ Mr. R. L. Wright) Washington, DC 20310
1	HQDA (DAEN-MCC-D, Mr. L. Foley) Washington, DC 20310
1	HQDA (DAEN-RDL, Mr. Simonini Washington, DC 20310
1	HQDA (DAEN-RDZ-A, Dr. Choromokos) Washington, DC 20310
1	HQDA (DALO-SMA) ATTN: COL W. F. Paris II Washington, DC 20310
1	HQDA (DAMA-CSM-CA) Washington, DC 20310
1	HQDA (DAMA-AR; NCL Div) Washington, DC 20310

No. of Copies	Organization
1	HQDA (DAMA-NCC, COL R. D. Orton) Washington, DC 20310
1	HQDA (DAPE-HRS) Washington, DC 20310
3	Director Institute for Defense Analyses ATTN: Dr. H. Menkes Dr. J. Bengston Tech Info Ofc 1801 Beauregard St. Alexandria, VA 22311
1	Commander US Army Ballistic Missile Defense Systems Command ATTN: J. Veeneman P. O. Box 1500, West Station Huntsville, AL 35807
1	Director US Army Ballistic Missile Defense Systems Command Advanced Technology Center ATTN: M. Whitfield P. O. Box 1500 Huntsville, AL 35807-3801
2	Director US Army Engineer Waterways Experimental Station ATTN: WESNP K. Davis P. O. Box 631 Vicksburg, MS 39180-0631
1	Commander US Army Materiel Command ATTN: AMCDRA-ST 5001 Eisenhower Avenue Alexandria, VA 22333-0001

DISTRIBUTION LIST

No. of Copies	Organization
1	Commander US Army Materiel Command ATTN: AMCSF 5001 Eisenhower Avenue Alexandria, VA 22333-0001
2	Commander US Army Armament Material Readiness Command ATTN: Joint Army-Navy-Air Force Conventional Ammunition Prof Coord GP/EI Jordan Rock Island, IL 61299
1	Commander Armament RD&E Center US Army AMCCOM ATTN: SMCAR-MSI Picatinny Arsenal, NJ 07806-5000
2	Commander Armament RD&E Center US Army AMCCOM ATTN: SMCAR-TDC SMCAR-LCM-SPC Picatinny Arsenal, NJ 07806-5000
1	Commander US Army Development and Employment Agency ATTN: MODE-ORO Fort Lewis, WA 98433-5000
1	Commander US Army Armament, Munitions and Chemical Command ATTN: AMSMC-IMP-L Rock Island, IL 61299-7300
1	Commander Pine Bluff Arsenal Pine Bluff, AR 71601
1	Commander CECOM R&D Technical Library ATTN: AMSEL-IM-L (Reports Section) B. 2700 Fort Monmouth, NJ 07703-5000
1	Commander US Army Rock Island Arsenal Rock Island, IL 61299
1	Commanding General US Army Armament Command ATTN: AMSAR-SA Rock Island Arsenal Rock Island, IL 61201
1	Commander US AMCCOM ARDEC CCAC Benet Weapons Laboratory ATTN: SMCAR-CCB-TL Watervliet, NY 12189-4050
1	Commander US Army Aviation Systems Command ATTN: AMSAV-ES 4300 Goodfellow Blvd. St. Louis, MO 63120-1798
1	Director US Army Aviation Research and Technology Activity Ames Research Center Moffett Field, CA 94035-1099
2	Director Lewis Directorate US Army Air Mobility Research and Development Laboratory Lewis Research Center ATTN: Mail Stop 77-5 21000 Brookpark Road Cleveland, OH 44135

DISTRIBUTION LIST

No. of Copies	Organization
1	Commander ATTN: AMSEL-IM-L (Reports Section) B. 2700 Fort Monmouth, NJ 07703-5000
1	Commander US Army Harry Diamond Lab. ATTN: SLCHD-TI 2800 Powder Mill Road Adelphi, MD 20783-1197
1	Commander US Army Missile Command Research, Development, and Engineering Center ATTN: AMSMI-RD-CS-R (Doc) Redstone Arsenal, AL 35898-5241
1	Director US Army Missile and Space Intelligence Center ATTN: AIAMS-YDL Redstone Arsenal, Al 35898-5500
1	Commander US Army Natick Research and Development Laboratories ATTN: AMDNA-D, Dr. D. Seiling Natick, MA 01760
1	Commander US Army Tank Automotive Command ATTN: AMSTA-TSL Warren, MI 48397-5000
1	US Army Engineer Division ATTN: Mr. Char P. O. Box 1600 Huntsville, AL 35807
1	Commandant US Army Engineer School ATTN: ATSE-CD Fort Belvoir, VA 22060
1	Commander Dugway Proving Ground ATTN: STEDP-TO-H, Mr. Miller Dugway, UT 84022
1	US Army Foreign Science and Technology Center ATTN: Research & Data Branch Federal Office Building 220-7th Street, NE Charlottesville, VA 22901
1	Commander Naval Weapons Center ATTN: Code 0632, Mr. G. Ostermann China Lake, CA 93555
1	Commander US Army Laboratory Command Materials Technology Laboratory ATTN: AMXMR-ATL Watertown, MA 02172-0001
1	Commander US Army Research Office P. O. Box 12211 Research Triangle Park, NC 27709-2211
1	Commander Naval Weapons Evaluation Facility ATTN: Document Control Kirtland AFB Albuquerque, NM 87117
1	Commander Naval Research Laboratory ATTN: Code 2027, Tech Lib Washington, DC 20375
1	Air Force Systems Command ATTN: IGFG Andrews AFB Washington, DC 20334
3	Commander US Army Belvoir Research and Development Center ATTN: STRBE-NN Fort Belvoir, VA 22060-5606

DISTRIBUTION LIST

No. of Copies	Organization
1	Assistant Secretary of the Navy (Research and Development) Navy Development Washington, DC 20350
1	Air Force Armament Laboratory ATTN: AFATL/DOIL (Technical Information Center) Eglin AFB, Fl 32542-5438
1	Commander Naval Surface Weapons Center Dahlgren Laboratory ATTN: E-23, Mr. J. J. Walsh Dahlgren, VA 22448
2	Commander Naval Surface Weapons Center White Oak Laboratory ATTN: R-15, Mr. M. M. Swisdak Mr. W. D. Smith III Silver Spring, MD 20902-5000
3	AFML (LNN, Dr. T. Nicholas; MAS; MBC, Mr. D. Schmidt) Wright-Patterson AFB, OH 45433
1	Headquarters Department of Energy Office of Military Application Washington, DC 20545
1	Mr. Richard W. Watson Director, Pittsburgh Mining & Safety Research Center Bureau of Mine, Dept of the Interior 4800 Forbes Avenue Pittsburgh, PA 15213
1	Director Lawrence Livermore Laboratory Technical Information Division P. O. Box 808 Livermore, CA 94550
1	Director Los Alamos Scientific Lab ATTN: Dr. J. Taylor P. O. Box 1663 Los Alamos, NM 87544
2	Director Sandia National Laboratories ATTN: Info Dist Div Dr. W. A. von Riesemann (Div 6442) Albuquerque, NM 87115
1	Director National Aeronautics and Space Administration George C. Marshall Space Flight Center Huntsville, Al 35812
1	Director National Aeronautics and Space Administration Scientific and Technical Information Facility P. O. Box 8757 Baltimore/Washington International Airport, MD 21240
1	National Academy of Science ATTN: Mr. D. G. Groves 2101 Constitution Avenue, NW Washington, DC 20418
10	Central Intelligence Agency OIR/DB/Standard GE47 HQ Washington, DC 20505
1	DNA Information and Analysis Center Kaman Tempo ATTN: DASOAC 816 State Street P. O. Drawer QQ Santa Barbara, CA 93102

DISTRIBUTION LIST

No. of Copies	Organization
1	Aberdeen Research Center ATTN: Mr. John Keefer 30 Diamond St. P. O. Box 548 Aberdeen, MD 21001
1	Agbabian Associates ATTN: Dr. D. P. Reddy 250 N. Nash Street El Segundo, CA 90245
1	Ammann & Whitney ATTN: Mr. N. Dobbs Suite 1700 Two World Trade Center New York, NY 10048
1	Black & Veatch Consulting Engineers ATTN: Mr. H. L. Callahan 1500 Meadow Lake Parkway Kansas City, MO 64114
1	Dr. Wilfred E. Baker Wilfred Baker Engineering P. O. Box 6477 San Antonio, TX 78209
1	Aeronautical Research Associates of Princeton, Inc. ATTN: Dr. C. Donaldson 50 Washington Road, P. O. Box 2229 Princeton, NJ 08540
1	Applied Research Associates, Inc. ATTN: Mr. J. L. Drake 1204 Openwood Street Vicksburg, MS 39180
1	J. G. Engineering Research Associates 3831 Menlo Drive Baltimore, MD 21215
1	McDonnell Douglas Astronautics Western Division ATTN: Dr. Lea Cohen 5301 Bosla Avenue Huntington Beach, CA 92647
1	Physics International 2700 Merced Street San Leandro, CA 94577
1	R&D Associates ATTN: G. P. Ganong P. O. Box 9335 Albuquerque, NM 87119
2	The Boeing Company Aerospace Division ATTN: Dr. Peter Grafton Dr. D. Strome Mail Stop 8C-68 P. O. Box 3707 Seattle, WA 98124
2	AVCO Corporation Structures and Mechanics Dept. ATTN: Dr. William Broding Dr. J. Gilmore 201 Lowell Street Wilmington, MA 01887
1	Aerospace Corporation P. O. Box 92957 Los Angeles, CA 90009
1	General American Transportation Corp. General American Research Div. ATTN: Dr. J. C. Shang 7449 N. Natchez Avenue Niles, IL 60648
1	Lovelace Research Institute ATTN: Dr. E. R. Fletcher P. O. Box 5890 Albuquerque, NM 87115

DISTRIBUTION LIST

No. of Copies	Organization
1	Science Applications, Inc. Suite 310 1216 Jefferson Davis Highway Arlington, VA 22202
2	Battelle Memorial Institute ATTN: Dr. L. E. Hulbert Mr. J. E. Backofen, Jr. 505 King Avenue Columbus, OH 43201
1	Georgia Institute of Tech ATTN: Dr. S. Atluri 225 North Avenue, NW Atlanta, GA 30332
1	IIT Research Institute ATTN: Mrs. H. Napadensky 10 West 35 Street Chicago, IL 60616
2	Southwest Research Institute ATTN: Dr. H. N. Abramson Dr. U. S. Lindholm 8500 Culebra Road San Antonio, TX 78228
1	Brown University Division of Engineering ATTN: Prof. R. Clifton Providence, RI 02912
1	Florida Atlantic University Dept. of Ocean Engineering ATTN: Prof. K. K. Stevens Boca Raton, FL 33432
1	Texas A&M University Department of Aerospace Engineering ATTN: Dr. James A. Stricklin College Station, TX 77843
1	University of Alabama ATTN: Dr. T. L. Cost P. O. Box 2908 University, AL 35486

No. of Copies	Organization
1	Director US Army TRADOC Analysis Command ATTN: ATAA-SL White Sands Missile Range, NM 88002-5502
1	Commandant US Army Infantry School ATTN: ATSH-CD-CSO-OR Fort Benning, GA 31905-5660
1	AWFL/SUL Kirtland AFB, NM 87117-5800
1	Air Force Armament Laboratory ATTN: AFATL/DLODL Eglin AFB, Fl 32542-5000
1	HQDA (SARD-TR) Washington, DC 20310-0001
1	Commander US Army Laboratory Command ATTN: AMSLC-DL Adelphi, MD 20783-1145
1	Director Benet Weapons Laboratory Armament RD&E Center US Army AMCCOM ATTN: SMCAR-LCB-TL Watervliet, NY 12189-4050
1	Commander US Army Armament, Munitions and Chemical Command ATTN: SMCAR-ESP-L Rock Island, IL 61299-5000
1	Commander US Army Aviation Systems Command ATTN: AMSAV-DACL 4300 Goodfellow Blvd. St. Louis, MO 63120-1798

DISTRIBUTION LIST

No. of Copies	Organization
1	Commander US Army Tank Automotive Command ATTN: AMSTAA-TSL (Technical Library) Warren, MI 48397-5800

Aberdeen Proving Ground

Dir, USAMSAA
ATTN: AMXSY-D
AMXSY-MP, H. Cohen
Cdr, USATECOM
ATTN: AMSTE-SI-F
AMSTE-TO-F
Cdr, CRDC, AMCCOM
ATTN: SMCCR-RSP-A
SMCCR-MU
SMCCR-MSI
Cdr, US Army Toxic and Hazardous Materials Agency
ATTN: AMXTH-TE

USER EVALUATION SHEET/CHANGE OF ADDRESS

This laboratory undertakes a continuing effort to improve the quality of the reports it publishes. Your comments/answers below will aid us in our efforts.

1. Does this report satisfy a need? (Comment on purpose, related project, or other area of interest for which the report will be used.) _____

2. How, specifically, is the report being used? (Information source, design data, procedure, source of ideas, etc.) _____

3. Has the information in this report led to any quantitative savings as far as man-hours or dollars saved, operating costs avoided, or efficiencies achieved, etc? *If so, please elaborate.* _____

4. General Comments. What do you think should be changed to improve future reports? (Indicate changes to organization, technical content, format, etc.) _____

BRL Report Number _____ Division Symbol _____

Check here if desire to be removed from distribution list. ____

Check here for address change. ____

Current address: Organization _____
Address _____

----------FOLD AND TAPE CLOSED----------

Director
U.S. Army Ballistic Research Laboratory
ATTN: SLCBR-DD-T(NEI)
Aberdeen Proving Ground, MD 21005-5066

OFFICIAL BUSINESS
PENALTY FOR PRIVATE USE $300

BUSINESS REPLY LABEL
FIRST CLASS PERMIT NO. 12062 WASHINGTON D.C.
POSTAGE WILL BE PAID BY DEPARTMENT OF THE ARMY

NO POSTAGE NECESSARY IF MAILED IN THE UNITED STATES

Director
U.S. Army Ballistic Research Laboratory
ATTN: SLCBR-DD-T(NEI)
Aberdeen Proving Ground, MD 21005-9989